TRANSPORT OF NANOSCALE ZERO VALENT IRON IN HETEROGENEOUS SOILS: MODEL DEVELOPMENT AND SENSITIVITY STUDY

MD ABDULLAH ASAD

A THESIS SUBMITTED TO THE FACULTY OF GRADUATE STUDIES
IN PARTIAL FULFILLMENT OF THE REQUIREMENTS FOR THE DEGREE OF
MASTER OF APPLIED SCIENCE

GRADUATE PROGRAMME IN CIVIL ENGINEERING
YORK UNIVERSITY
TORONTO, ONTARIO

NOVEMBER 2018

ABSTRACT

Subsurface remediation using nanoscale zero valent iron (nZVI) is a promising in-situ technology that can convert groundwater contaminants into non-toxic compounds. Despite its promising characteristics, field scale implementation of nZVI technology has faced major challenges due to poor subsurface mobility and limited longevity, all leading to smaller nZVI travel distance. How far nZVI travels in the subsurface is an important parameter as it influences the amount of contaminants that could be reached and thereby remediated.

This thesis examined various factors (viscosity, groundwater velocity, injection flux, soil heterogeneity, lag period) on nZVI travel distance through a numerical model and by performing a statistical analysis which revealed that viscosity has a statistically significant impact on nZVI travel distance while the impact of groundwater velocity and injection flux are statistically insignificant. The model also revealed that soil heterogeneity plays an important factor and that longer nZVI injection periods are better for nZVI deployment in the field.

DEDICATION

To my beloved parents, and my lovely wife.

ACKNOWLEDGEMENTS

I have been fortunate enough to be supervised by Dr. Magdalena Krol, who is a great researcher and a very kind-hearted person. I really appreciate her continual support, feedback, and encouragement throughout my master's. Her guidance and suggestion have led me to shape this work.

I would like to thank Dr. Scott Briggs who supported me during my thesis with his great knowledge. His guidance and continual feedback helped me to implement this work. I am grateful to Dr. Usman Khan who provided advice and insight into the statistical approach of the thesis. I am very thankful to Dr. Pulin Mondal and Dr. Sunil Bisnath for their feedback and recommendations on my thesis. I am thankful to York University, all faculty members and non-faculty members. During my journey as a master's student, I have met many wonderful colleagues and friends. I am thankful to them.

I am forever indebted to my father who has encouraged me to believe in myself and built my confidence to complete this thesis and to my mother who struggled throughout her life to raise me to this position. I am also grateful to my parents-in-law for their continuous encouragement and prayers for my success.

Lastly, I want to thank my wife Mohona, who continuously supported me during times of frustration. She is the women behind this successful journey. I am really lucky to have her company and huge support during my studies.

TABLE OF CONTENTS

LIST OF TABLES

LIST OF FIGURES

NOMENCLATURE

Symbol

A	Hamaker constant (J)
Ag	Silver
A_S	Porosity dependent parameter $(-)$
C	Aqueous solute concentration $(mol.\,m^{-3})$
$\frac{C}{C_o}$	Relative nZVI concentration
C_{in}	Initial molar concentration of nZVI $(mol.\,m^{-3})$
C_{ip}	Initial molar concentration of polymer $(mol.\,m^{-3})$
C_I	nZVI injection concentration $(g.\,L^{-1})$
C_N	aqueous nZVI concentration
C_P	aqueous polymer concentration
Cu	Copper
D	Brownian diffusion
D_B	Bulk diffusion coefficient $(m^2.\,s^{-1})$
d_C	Collector (soil grain) diameter(m)
D_e	Effective diffusion coefficient $(m^2.\,s^{-1})$
D_{disp}	Effective hydrodynamic dispersion tensor $(m^2.\,s^{-1})$

D_F	Diffusion
D_{FN}	Diffusion coefficient of nZVI $(m^2.s^{-1})$
D_{FP}	Diffusion coefficient of polymer $(m^2.s^{-1})$
d_P	Diameter of nZVI (m)
D_P	Dispersion (m)
Fe^0	Zero valent iron
F_N	nZVI flux $(mol.m^{-2}.s^{-1})$
F_P	polymer flux $(mol.m^{-2}.s^{-1})$
g	Acceleration due to gravity $(m.s^{-2})$
G	Gamma $(-)$
H_0	Null hypothesis
H_A	Alternative hypothesis
I	Interception
I_{MNP}	Molar rate of injection of nZVI and polymer $(mol.kg^{-1})$
I_z^M	Second moment of the mass about the z axis $(m * mol)$
k	Boltzman constant (J/k)
k_{att}	Attachment rate coefficient (s^{-1}) in colloid filtration theory
$k_{att}C$	Attached concentration $(mol.m^{-3}s^{-1})$
K_d	Partitioning coefficient (m^3kg^{-1})

k_{det}	Detachment rate coefficient (s^{-1})
k_{ret}	Attachment/retention rate coefficient (s^{-1})
K_{eq}	Equilibrium constant $(-)$
k_P	Permeability of the aquifer porous media (m^2)
L	Length of domain (m)
$\log(\mu_p)$	Polymer viscosity $(Pa.s)$
M	Total mass of nZVI $(mol.m^{-3})$
(M_F)	Mass flux $(kg.m^{-2}.s^{-1})$
M_{WN}	Molecular weight of nZVI $(kg.mol^{-1})$
M_{WP}	Molecular weight of CMC polymer $(kg.mol^{-1})$
n	Vector normal to the boundary
N_A	Attraction number $(-)$
N_G	Gravity number $(-)$
N_{Pe}	Peclet number $(-)$
N_R	Aspect ratio $(-)$
N_{vdW}	Van der Wall's number $(-)$
Ni	Nickel
Pd	Palladium
Pt	Platinum

P_t	Percentage of nZVI or polymer in total solution $(\%)$
q	Groundwater velocity or Darcy velocity $(\mathrm{m.s^{-1}})$
Q_m	Sink/Source $(\mathrm{kg.m^{-3}s^{-1}})$
r_P	Colloid radius (m)
R_I	Radius of injection well (m)
S	Sorbed concentration $(\mathrm{kg.m^{-3}})$
S_T	Total attachment $(\mathrm{mol.kg^{-1}})$
t	Time (s)
T	Temperature (K)
v	Porewater velocity $(\mathrm{m.s^{-1}})$
x	Distance in x-direction (m)
x_{ij}	Value of random variable $(-)$
X_N	Mole fraction of nZVI $(\frac{\text{mol of nZVI}}{\text{mol of water}})$
x_{ni}	Initial mole fraction nZVI $(\frac{\text{mol of nZVI}}{\text{mol of water}})$
XCN	Horizontal center of mass (m)
$XNSP$	Spreading of the mass in horizontal direction (m)
X_P	Mole fraction of polymer $(\frac{\text{mol of polymer}}{\text{mol of water}})$
x_{pi}	Initial mole fraction CMC polymer $(\frac{\text{mol of polymer}}{\text{mol of water}})$

ZCN	Vertical center of mass (m)
ZNSP	Spreading of the mass in vertical direction (m)
θ	Porosity $(-)$
α	Attachment efficiency $(-)$
α_{L}	Longitudinal dispersity (m)
ϵ_{ij}	Random error component $(-)$
η_0	Single collector contact efficiency $(-)$
μ	Overall mean
μ_{nf}	Viscosity of nZVI $(\mathrm{Pa.s})$
μ_{p}	Polymer viscosity $(\mathrm{Pa.s})$
μ_{sol}	Solution viscosity $(\mathrm{Pa.s})$
μ_{sub}	Subsurface viscosity $(\mathrm{Pa.s})$
μ_{wf}	Water viscosity $(\mathrm{Pa.s})$
ρ_{F}	Water density $(\mathrm{kg.m^{-3}})$
ρ_{b}	Density of porous media $(\mathrm{kg.m^{-3}})$
τ_{i}	Factor effect
$\nabla \mathrm{h}$	Hydraulic gradient $(\mathrm{m.m^{-1}})$
$\nabla \mathrm{P}$	Pressure gradient

Subscripts

A	Attraction
B	Bulk
C	Collector
e	Effective
F	Fluid or solution
G	Gravity
I	Injection
L	Longitudinal
m	Mass
P	Particles or colloids
Pe	Peclet number
sub	Subsurface
vdW	Van der Wall's

Abbreviation

1D	One-dimensional
2D	Two-dimensional
3D	Three-dimensional

AD	Advection and diffusion-dispersion
ANOVA	Analysis of variance
BC	Boundary conditions
CF	Constant flux
CFT	Colloid filtration theory
CGS	Canadian Geotechnical Society
CH	Constant head
C_2H_6	Ethane
CMC	Carboxymethyl cellulose
CompSim	3D finite difference, three-phase, simulator
COMSOL	A finite element based Multiphysics simulation software
DL	Darcy's law module
DNAPL	Dense nonaqueous phase liquid
DO	Dissolved oxygen
EZVI	Emulsified nZVI
nZVI	Nanoscale zero valent iron
ORP	Oxidation reduction potential
PSS	Poly-styrene sulfonate
PAA	Polyacrylic acid

PCE, C_2Cl_4	Tetrachloroethylene
PPI	Pressure pulse injection
SS	Suspended solid
TCE	Trichloroethylene
TDS	Transport of Diluted Species Module
TS	Total solids

Chapter 1 Introduction

Groundwater contamination can be a result of chemicals such as heavy metals and chlorinated solvents making their way to underlying aquifers. This leads to environmental damage and potential health issues if such aquifers are used as a drinking water source (Harr 1996). In addition, as exposure to contaminated groundwater is dangerous, extracting it out of the ground surface for treatment is often risky (as some contaminants may cause health issues (Costas et al. 2002)) and costly. Therefore, innovative in situ technologies are required, preferably at the source zone (area where contamination originates from). One such technology is nanoscale zero valent iron (nZVI) which can be injected into the subsurface and has shown significant potential in remediating contaminated groundwater (O'Carrol et al 2013; Li et al. 2006).

In this chapter, an overview of the nZVI technology, the mobility of nano particles in the subsurface, and implementation challenges at the field scale are reviewed and described. Although many studies have been conducted in the laboratory, this chapter focuses on field-scale implementation. In addition, the objectives of the thesis are outlined.

1.1 Nanoscale Zero Valent Iron (nZVI) Technology

nZVI remediation works because the zero valent iron (Fe^0) releases an electron when it is oxidized. These electrons can then reduce organic groundwater

contaminants, through reductive dechlorination, converting them into non-toxic compounds (Li et al. 2006, O'Carroll et al. 2013). For example, tetrachloroethylene (PCE, C_2Cl_4) can be reduced to ethane (C_2H_6) (Eq. 1-1), which poses a little toxicological risk (Li et al. 2006).

$$C_2Cl_4 + 5Fe^0 + 6H^+ \rightarrow C_2H_6 + 5Fe^{2+} + 4Cl^- \qquad (\mathbf{1-1})$$

Inorganic contaminants such as hexavalent chromium (Cr^{6+}), divalent nickel (Ni^{2+}) and divalent lead (Pb^{2+}) can be reduced by nZVI to less toxic state as Cr^{3+}, $Ni^{0,}$ and Pb^0 respectively, adsorbed on the nZVI surface as Cr^{6+}, $Ni^{2+,}$ and Pb^{2+} and precipitated as oxides (O'Carroll et al. 2013). Figure 1 shows a remediation scenario using nZVI. Generally, nZVI is injected into subsurface through an injection well and as it moves through the subsurface it reacts with the contaminants, remediating the site. Alternatively, nZVI can be injected into the source zone but can be effected by source concentration, reactivity, and location (Taghavy et al. 2010).

When injected into the subsurface, nZVI particles may aggregate (formation of larger sized particles due to dominant attractive forces (Petosa et al. 2010)) which can limit their mobility and reactivity, therefore different kind of stabilizers and surface coatings have been used to increase nZVI stability in porous media. Some of these coatings include carboxymethyl cellulose (CMC), guar gum, poly-styrene sulfonate (PSS), an emulsion of biodegradable vegetable oil and water, and

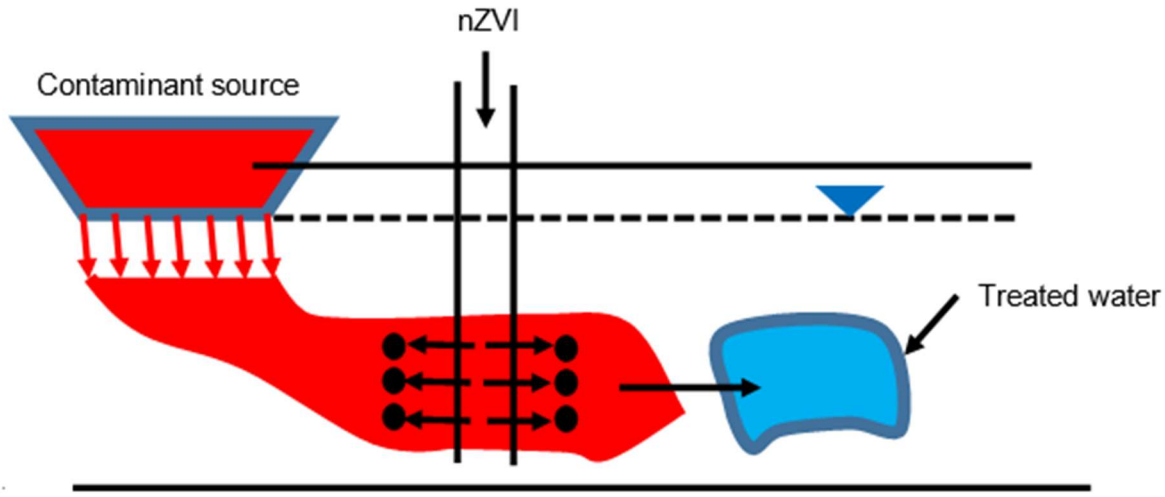

Figure 1.1: nZVI remediation schematic

polyacrylic acid (PAA) (Quinn et al. 2005, Lin et al. 2010, Raychoudhury et al. 2010, Sakulchaicharoen et al. 2010). These coatings can be applied on the iron surface during synthesis or after. In addition, bimetallic nZVI particles have been produced by modifying nZVI surfaces with noble metals (Elliott and Zhang 2001, Henn and Waddill 2006, Sakulchaicharoen et al. 2010). These noble metals can include Palladium (Pd), Platinum (Pt), Nickel (Ni), Silver (Ag), or Copper (Cu) and their addition increases the rate of reduction of contaminants (O'Carroll et al 2013).

1.2 nZVI Travel Distance in Groundwater

nZVI mobility and longevity are important parameters when implementing nZVI technology in the field. As seen from Figure 1.1, in order for nZVI to be successful it needs to travel from the injection well to the contaminants. Even if injected into the source zone, nZVI still needs to travel from the injection well to the outskirts of

the source zone to ensure complete remediation. However, various range of nZVI mobilities have been reported in different field studies based on different measurement strategies such as contaminant degradation efficiency in monitoring well, visual observation of compounds extracted from monitoring well, analysis of extracted groundwater, nZVI reduction efficiency, measurement of acidity or basicity (i.e., pH measurement) and measurement of dissolved oxygen (DO). In addition, nZVI longevity (how long nZVI stays active and does not react with non-contaminants) also varies in literature. In general, nZVI can be injected into the subsurface using gravity fed (constant head) or constant flux methods. Gravity fed injections specify a constant pressure or head that controls the flow, while constant flux uses a constant flow rate for injection.

Gravity fed injections have been used by many ((Elliott and Zhang 2001, Kocur et al, 2014, Zhang 2003, Wei et al, 2010, Henn and Waddill, 2006; Chowdhury et al, 2015) to introduce nZVI into the subsurface. Elliott and Zhang (2001) injected nanoscale bimetallic Fe-Pd particles by gravity fed injection in an unconfined saturated aquifer for two days to remediate groundwater contaminated by trichloroethylene (TCE) and chlorinated aliphatic hydrocarbons. These particles were reported to travel at least 1.5 m based on the observed maximum degradation in the closest piezometer location. Zhang (2003) documented a test done by Glazier et al. (2003) in the Durham sub basin, North Carolina, where slurry of potable water and nZVI particles were freshly prepared on site and injected by

gravity with the help of a submersible pump. They reported a 6 to 10 m radius of influence of injected nZVI particles based on notable reduction in contaminant concentration. Elliott and Zhang (2001) used a recirculation system during gravity fed injection of bimetallic Fe-Pd particles and high contaminant reduction was observed at the injection well and adjacent piezometer spaced at 1.5 m. The recirculation system has also been used in other field studies (Henn and Waddill 2006, Chowdhury et al. 2015, Kocur et al. 2014). Basically, the system involved extracting contaminated groundwater to be mixed with particles before injection, allowing for pre-treatment of contamination. Henn and Waddill (2006) reported nZVI travel distance of 6 m as nZVI migrated to a downgradient well during gravity fed injection and visual observation in several extraction wells reported cloudy/black strained water indicating the presence of nZVI colloids. Wei et al. (2010) injected freshly prepared Fe-Pd particles into a contaminated site by gravity fed injection and reported a 3 m distance measured by suspended solid (SS) and total solid (TS) analysis. They compared the mobility of this freshly prepared Fe-Pd suspension with commercially available Fe-Pd suspension and opined that freshly prepared suspension has better mobility. Kocur et al. (2014) reported at least 1 m travel distance of CMC-nZVI particles to a downgradient monitoring well in a contaminated sandy soil during gravity fed injection. Chowdhury et al (2015) used a peristaltic pump to inject CMC-nZVI by gravity into a variably saturated shallow aquifer and found particles to travel at least 0.8 m away from well, based

on indirect measurements such as oxidation-reduction potential (ORP), pH and DO.

He et al. (2010) combined gravity fed and constant flux (pressure injection) methods using a peristaltic pump to inject CMC stabilized Fe-Pd particles in a contaminated unconfined aquifer. The peristaltic pump maintained a constant head for gravity fed while during pressure injection the well head was sealed, and a pressure gauge was installed with a total pressure of less than 5 psi. They reported more nZVI mobility during high pressure injection than during gravity fed injections, where particles travelled up to 3 m down gradient.

Constant flux injection has been modified in different field injections using several techniques. One such technique is pressure pulse injection (PPI) where an injection tool is attached with an inflatable packer that isolates the target injection area and then particles are pushed by a perforated injection pipe with large-magnitude pressure pulses. This technique was used by Quinn et al. (2005) to remediate contaminated groundwater by injecting emulsified (emulsion of biodegradable vegetable oil and water) nZVI (EZVI) into eight wells located in a dense non-aqueous phase liquid (DNAPL) source zone. DNAPLs are liquids that are denser than water with low water solubilities, such as PCE, trichloroethylene (TCE), polychlorinated biphenyl (PCB), coal tar, mercury and extra heavy crude oil (National Research Council, 1999). Although the authors did not report any exact

distance travelled by EZVI, they did find that EZVI did not travel the expected distance.

Another technique is pneumatic fracturing used by Su et al. (2013) to inject EZVI by injecting nitrogen gas first followed by EZVI injection. This type of injection was compared to direct, or constant flux injection and showed that pneumatic injection resulted in higher EZVI travel distance. For an example, Su et al. (2013) reported a 2.1 m travel distance for EZVI colloids during pneumatic injection compared to 0.89 m for direct injection.

Bennett et al. (2010) found that CMC-nZVI were mobile in the subsurface but their mobility was reduced with time and became immobilized after 13 hours and transport ranges varied from 0.54 m to 1.3 m in several direct push and pull tests. Busch et al. (2015) reported nZVI travel distance up to 5.3 m during constant flux injection while 12 % of the particles were found in this distance and significant amount decreased before this due to deposition in porous media. It should be noted that seepage velocity was 2 $(\mathrm{m.h^{-1}})$ and the injection rate was 500 $(\mathrm{L.h^{-1}})$. This high injection rate may be attributed to the increased travel distance because most of the studies used injection rate lower than this value, (i.e., Bennett et al. (2010) used a maximum of 318 $(\mathrm{L.h^{-1}})$ (5.3 $\mathrm{L.min^{-1}}$).

In most cases, the injection of nZVI using gravity fed methods resulted in shorter travel distances due to lowered injection velocities (compared to constant flux injections), especially if polymer-stabilized nZVI were used. This shorter travel

distance is due to viscosity effects and increased attachment rates at lower velocities (Krol et al, 2013). In addition, mobility can be enhanced using recirculation techniques or flushing with water or stabilizing solution (Henn and Waddill 2006, Chowdhury et al. 2015, Mondal et al. 2018). Conversely, incorporating lag times in the injection strategy can decrease nZVI mobility as the reduced average velocity may result in attachment onto soil grains (Bennet et al, 2010; Krol et el, 2013).

Although nZVI mobility is the focus of most remediation studies (due to the importance of the particles reaching the contaminants), most field and lab applications report moderate mobility ranging from 1 to 6 m (Kocur et al, 2014; Elliott and Zhang, 2001; Henn and Waddill, 2006; Zhang, 2003; Köber et al. (2014). In addition, the reported nZVI travel distance is often measured by visual sightings of nZVI with distance, examining contaminant concentration downgradient of the injection well or by indirect measurements such as change in ORP, SS, and TS analysis etc.

Although numerous studies have been performed, as outlined above, transport behavior of nZVI in the subsurface is still not well understood. One thing that is common among all the studies is that they all agree that optimum travel distance for successful remediation has not been achieved yet. In addition, the effect of various factors has not been systematically studied and comparison of various studies is difficult due to the change in system parameters. From the

studies outlined above, nZVI transport distances range depends on injection types, injection rates, injection strategy (e.g., lag period, circulation), mass injected, the viscosity of injected solution, and the type of particle used. However, the factor has the most effect on nZVI travel distance has not been identified.

1.3 Implementation Challenges of nZVI Remediation

Despite its promising characteristics, field scale implementation of nZVI technology has faced major challenges due to poor subsurface mobility, limited longevity (O'Carroll et al. 2013, Kocur 2015), and well clogging (Elliott and Zhang 2001), all leading to a smaller travel distance. A larger travel distance is preferable since it can reduce the total time of remediation and provide a cost-effective solution. There are several factors which may have an effect on nZVI travel distance.

1.3.1 Factors Affecting nZVI Travel Distance

Research has been carried out by others to identify the factors which may have an effect on particle travel distance. nZVI travel distance may be affected by rapid aggregation, settling, oxidation, nZVI injection method, groundwater/porewater velocity, injection flux, lag phase (time duration when nZVI injection is stopped), solution viscosity, and subsurface heterogeneity (Bennett et al. 2010, Krol et al. 2013, Raychoudhury et al. 2014, Kocur et al. 2014).

Aggregation may occur due to particle-particle interaction (Petosa et al. 2010) and settling occurs due to gravitational forces (Phenrat et al. 2007). These factors affect nZVI travel distance by reducing the amount of nZVI particles available for transport (O'Carroll et al. 2013, Raychoudhury et al. 2014, Kocur 2015).

The method of nZVI injection may also influence nZVI travel distance. As mentioned above, different types of injection strategies can be used for nZVI remediation. These include pneumatic injection, direct injection, pressure pulse injection, gravity fed injection etc. (Su et al. 2013, Kocur et al. 2014). While gravity fed injection generally maintains a constant head at the injection well, other injection methods depend on injecting flux in the porous media. Krol et al. (2013) considered both constant flux (CF) and constant head (CH) injections from field injection data of (Bennett et al. 2010) in a three-dimensional (3D) numerical model and found a higher travel distance in the case of a CF injection.

Laumann et al. (2013) conducted a column experiment for nZVI transport and suggested that doubling the injection velocity increased nZVI transport (Breakthrough of PAA-nZVI rose from 0.32 to 0.70). According to Kocur et al. (2014), field nZVI travel distance and longevity can be achieved with very high porewater velocity and highly stable nZVI suspension. Alternatively, lag phase during successive nZVI injection can lead to nZVI deposition in porous media

under low porewater velocity condition (Bennett et al. 2010, Kocur et al. 2014) and make nZVI immobile (Krol et al. 2013).

nZVI travel distance can also be influenced by the solution viscosity (Krol et al. 2013, Chowdhury et al. 2015). nZVI solution viscosity and stability can be increased by adding different types of polymer such as CMC (Li et al. 2015). Li et al. (2016) observed greater travel efficiency (38% mass eluted) by adding 2 $\mathrm{g.L^{-1}}$ CMC compared to 1 $(\mathrm{g.L^{-1}})$ (11% mass eluted) at a fixed nZVI concentration. Higher nZVI recovery was observed from the experimental sand tank as CMC concentration was increased from 1 to 2 $(\mathrm{g.L^{-1}})$. However, increasing solution viscosity decreased the hydraulic conductivity, lowering the travel velocity (as hydraulic conductivity is inversely proportional to viscosity and proportional to Darcy velocity (De Wiest 1966)) and hence the travel distance (Mondal et al. 2018).

nZVI concentration in the injected solution can also affect nZVI travel distance. Laboratory experiments showed a higher fraction of nZVI was recovered by injecting lower concentrations (Phenrat et al. 2010, Li et al. 2016). However, the length of the sand-tank was fixed during the experiment therefore the actual nZVI travel distance directly could not be obtained.

Lastly, subsurface heterogeneity can affect nZVI travel distance. For example, more nZVI can be transported in coarse sands than in fine sands (Yang et al. 2007, Phenrat et al. 2010, Raychoudhury et al. 2014, Li et al. 2016) and during various field injections, subsurface heterogeneity was found to strongly

hinder transport (Kocur et al. 2014) and distribution of nZVI (Henn and Waddill 2006). In addition, preferential flow caused by subsurface heterogeneity can negatively impact the remediation goals as nZVI fails to reach the target contaminant (He et al. 2010, Velimirovic et al. 2014). Daylighting of injected solution (when the solution shows up on the surface) was also observed in a field study (Su et al. 2013). In addition, phenomenon such as aggregation is greatly influenced by soil particle size.

As natural aquifers are heterogeneous in nature, modeling studies should incorporate heterogeneity (variable permeability field in the subsurface aquifer) to investigate its effect and understand the possible consequences. There are few modeling studies that simulated heterogeneity of soils. Cullen et al. (2010) simulated the transport of carbon nanoparticles in heterogeneous permeability field and opined that less movement of nanoparticles happens in a heterogeneous media compared to homogeneous media. Strutz et al. (2016) predicated that nZVI particles will be retained on high permeability areas after initial transport in a heterogeneous media. Most recently, Mondal et al. (2018) compared experimental transport of CMC-nZVI with the model result in a heterogeneous domain (variable permeability in clean silica sand). They investigated the impact of solution viscosity, porewater velocity of flushing distilled water, nZVI attachment efficiency on nZVI concentration and found that lower viscosity, lower attachment efficiency, and higher porewater velocity cause high nZVI concentration in the domain.

Although these studies have investigated the role of heterogeneity and sensitivity of some factors on nanoparticles and nZVI transport through laboratory and numerical studies, no studies have investigated the statistically significant impact of possible factors on nZVI transport in heterogeneous groundwater aquifer representing field aquifer conditions.

1.3.2 Factors Affecting nZVI Longevity

Unwanted nZVI oxidation with oxidants that are not contaminants (i.e., DO, water, natural oxidants) is responsible for limited nZVI longevity/lifetime in groundwater (Su et al. 2013, Kocur 2015). In this case, instead of reacting with contaminants, nZVI is oxidized mostly by DO in groundwater which eventually forms various iron products (magnetite and other iron oxides) (Su et al. 2013) and results in nZVI loss. This factor affects nZVI travel distance by reducing the active iron content.

1.4 Thesis Objectives

The literature review reveals that there are few modeling studies done taking soil heterogeneity in subsurface into account. Such a study may bridge the gap in fundamental understanding of nZVI transport in groundwater and help in overcoming the implementation challenges at the field scale. As such, this study examines factors that will have the greatest impact on nZVI travel distance, taking soil heterogeneity into consideration. There are three specific objectives of this thesis:

1. To identify factors that affect nZVI travel distance and hence, groundwater remediation through a literature study.
2. To develop a field-validated 3D model for nZVI transport in the subsurface.
3. To perform a sensitivity analysis to identify which factors that have the most impact on nZVI transport on soils with various ranges of heterogeneity, using the analysis of variance (ANOVA).

The first objective has been addressed in Chapter 1. Literature has been reviewed in this chapter to identify the parameters/factors which may have an impact on nZVI technology with respect to travel distance and groundwater remediation. Chapter 2 delves a bit deeper into some of these effects, as well as, the theory behind nZVI transport.

Chapters 3 and 4 deal with the second objective. A 3D model has been developed using COMSOL (a software platform based on finite element analysis), by modifying the colloid filtration theory (CFT) and verifying it with a field validated model developed by Krol et al. (2013).

Chapter 5 deals with the third objective. Using the validated model, a two-dimensional (2D) statistical analysis has been performed on the effect of various important nZVI factors, including groundwater velocity, solution viscosity, and injection flux. ANOVA was used on two sets of subsurface permeability realizations representing two aquifers with varying levels of heterogeneity, and the sensitivity of mass distribution in the subsurface was examined.

Chapter 2 Theory on Fate and Transport of Colloid in Porous Media

In this chapter, the governing equations for nZVI transport are described. These include: the advection-dispersion (AD) equation, physicochemical filtration of colloids in porous media including the CFT, the Darcy law for flow through porous media and the relationship between soil grain size and permeability in a heterogeneous domain.

2.1 Nanoparticle Transport

To simulate nZVI transport in the subsurface, the AD equation can be modified for colloidal transport, described in section 2.2 (Frimmel et al. 2007, Alonso et al. 2007). The transport of nZVI in the aqueous phase in a homogenous granular porous media can be defined by AD equation (given in the general form (Eq. 2-1a) and one-dimension form (Eq. 2-1b)) (Schijven and Hassanizadeh 2000, Tufenkji 2007):

$$\frac{\partial \mathrm{C}}{\partial \mathrm{t}}\theta = -\nabla \cdot (\vec{\mathrm{q}}\mathrm{C}) + \theta \mathrm{D}_{\mathrm{disp}} \nabla^2 \mathrm{C} \qquad (\mathbf{2-1a})$$

$$\frac{\partial \mathrm{C}}{\partial \mathrm{t}}\theta = -\vec{\mathrm{q}}\frac{\partial \mathrm{C}}{\partial \mathrm{x}} + \mathrm{D}_{\mathrm{disp}}\frac{\partial^2 \mathrm{C}}{\partial \mathrm{x}^2}\theta \qquad (\mathbf{2-1b})$$

Where C is the aqueous nZVI concentration$(\mathrm{mol.m^{-3}})$ at a distance of x (m) and time $\mathrm{t}\,(\mathrm{s})$, θ is the porosity $(-)$, q is the Darcy velocity $(\mathrm{m.s^{-1}})$ $(\mathrm{q} = \theta \mathrm{v}$

where v is the porewater velocity $(m.s^{-1})$. D_{disp} is the effective hydrodynamic dispersion coefficient $(m^2.s^{-1})$.

2.1.1 Advection

Advection is the transport of solutes due to porewater velocity or plug flow (Fetter et al. 1993). It is the dominant transport mode for aqueous phase species (Steefel and Lasaga 1992). The term $\nabla \cdot (\vec{q}C)$ in Eq. (2-1a) represents advective transport.

2.1.2 Effective Dispersion

The term $D_{disp}\nabla^2 C$ in Eq. (2-1) represents effective dispersive transport. This term is a combination of diffusion and dispersion (Fetter et al. 1993):

$$D_{disp} = D_e + \alpha_L v \qquad (\mathbf{2-2})$$

where D_e is the effective diffusion coefficient $(m^2.s^{-1})$ and α_L is the longitudinal dispersivity (m). Diffusion is the spreading of solutes due to a concentration gradient (Fetter et al. 1993). Diffusion is typically a much slower mechanism than advection but in soils such as clays and silts, where advective flux is low, diffusion may become the dominant transport mechanism (Rudolph et al. 1991).

Dispersion describes solutes spreading due to variation in velocity from pore to pore. This can be the result of geological heterogeneities and local flow patterns (Fetter et al. 1993).

Colloid transport in porous media is not only governed by advection, diffusion, and dispersion but also deposition of colloids as they move. Therefore, the AD equation cannot sufficiently predict colloid behaviour, as it only describes the behaviour of the aqueous nZVI phase and removal process in porous media as physiochemical filtration is not considered (Molnar et al. 2015). Since nZVI is considered a colloid, the AD equation was modified with the CFT equation to accurately describe nZVI transport in subsurface porous media.

2.2 Physiochemical Filtration of Colloids in Porous Media

Physiochemical filtration of colloids has been described as both reversible and irreversible phenomena (Tufenkji 2007). Reversible processes have been described by both equilibrium adsorption and kinetic adsorption-desorption while irreversible processes have been defined by CFT.

2.2.1 Equilibrium Adsorption

Equilibrium adsorption or attachment of colloids from the aqueous phase to the solid phase can be defined as follows (Tufenkji 2007):

$$S = K_{eq} C \qquad (\mathbf{2-3})$$

Where S is the sorbed concentration $(\mathrm{kg.\,m^{-3}})$, C is the concentration in the aqueous phase $(\mathrm{mol.\,m^{-3}})$ and K_{eq} is the equilibrium constant $(\mathrm{kg.\,mol^{-1}})$. Equilibrium adsorption is considered to be non-reversible (no desorption).

2.2.2 Kinetic Adsorption-Desorption

This theory assumes that adsorption (attachment) and desorption (detachment) are governed by a kinetic, reversible process before equilibrium is established in the system. Attachment happens when colloid (or other compound) contacts the solid surface and get adsorbed onto it due to physiochemical interplay (Tufenkji 2007). Detachment happens when colloids detach from the soil surface (Tufenkji 2007).

The net changes in attached concentration can be defined as follows (Tufenkji 2007):

$$\frac{\rho_b}{\theta}\frac{\partial S}{\partial t} = k_{ret}C - \frac{\rho_b}{\theta}k_{det}S \qquad (\mathbf{2-4})$$

Where ρ_b is the density of porous media $(kg.m^{-3})$, k_{ret} is the attachment/retention rate coefficient (s^{-1}) and k_{det} is the detachment rate coefficient (s^{-1}).

Sorption represents the partitioning of solute between solution and solids. The overall sorption process can also be defined as follows (Wang et al. 2009):

$$\frac{\rho_b}{\theta}\frac{\partial S}{\partial t} = \frac{\rho_b}{\theta}\frac{\partial S}{\partial C}\frac{\partial C}{\partial t} = \frac{\rho_b}{\theta}K_d\frac{\partial C}{\partial t} \qquad (\mathbf{2-5})$$

Where the term K_d is the partitioning coefficient $(m^3.kg^{-1})$ that represents the partitioning of the solute $(\frac{\partial S}{\partial C})$ between solution and solids during the sorption process (Wang et al. 2009). This is a reversible process and can be incorporated into the one dimensional (1D) AD equation as follows:

$$\frac{\partial C}{\partial t}\theta = -q\frac{\partial C}{\partial x} + D_{disp}\frac{\partial^2 C}{\partial x^2}\theta - K_d\frac{\partial C}{\partial t}\rho_b \qquad (\mathbf{2-6})$$

According to Schijven and Hassanizadeh (2000), both equilibrium adsorption and kinetic adsorption-desorption methods may provide the same conclusions and are not appropriate to describe colloid transport.

2.2.3 Sorption Process vs. Filtration Process

The breakthrough curves show the normalized concentration $(\frac{C}{C_0})$ with pore volumes and allow comparison of various transport mechanisms such as sorption and filtration (Kirkham 2014). Figure 2.1 demonstrates the general differences between 'classical' filtration versus sorption (Molnar et al. 2015). The transport of a non-reacting tracer is normally defined by the AD equation not considering retardation in the porous media, therefore, the breakthrough curve is fast and reaches initial concentrations (Figure 2.1a). On the other hand, transport of reactive solute in porous media considers retardation (Eq. 2-6) due to partitioning effect (both attachment/adsorption and detachment/desorption in porous media). The resulting breakthrough curve still reaches initial concentrations but a lag (retardation) is observed when compared to the non-reactive tracer (Figure 2.1b). For colloids, filtration is a kinetic process where attachment happens much faster than detachment (colloid detaching from the collector surface and re-entering the bulk pore fluid) (Schijven and Šimůnek 2002, Tufenkji 2007).

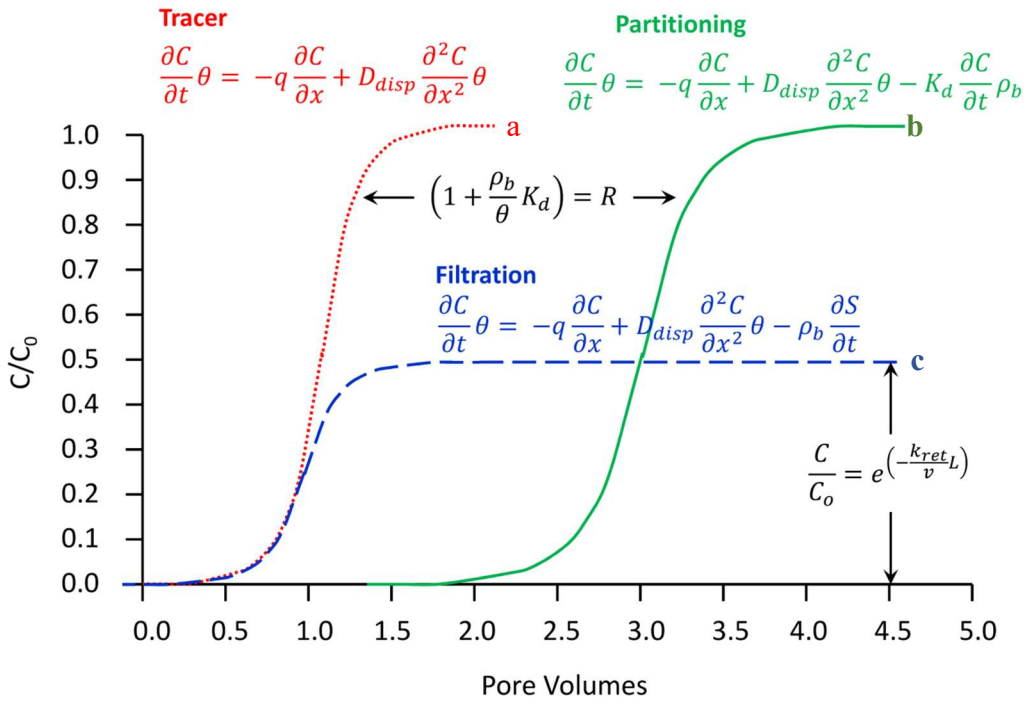

Figure 2.1: Conservative non-reacting tracer (a - dotted red line), partitioning (b - solid green line), and filtration (c - dashed blue line) breakthrough curves. Where L is the distance travelled, R is the retardation factor, C_0 is the initial (influent) concentration. All other symbols are as previously defined in the text. Reproduced with permission from (Molnar et al. 2015).

Colloid filtration considers the attachment process which is irreversible (detailed description in the next section 2.2.4), which is why the breakthrough curve for filtration is lower than the other breakthrough curves (i.e., tracer and solute) but appears at the same time as the non-reactive tracer (Figure 2.1c).

2.2.4 Colloid Filtration Theory

CFT was developed by Yao et al. (1971) and is the most common approach for colloid transport modeling both at laboratory and field scales. CFT describes an irreversible two-step attachment process where a single collector represents a soil grain (Figure 2.2).

Step 1. Colloids come into contact with the collector surface by mechanisms such as Brownian diffusion (D), interception (I) and gravitational sedimentation (G). The ratio of colloids hitting the collector to those approaching the collector is described by the single collector contact efficiency, η_0 .

Step 2. A fraction of the colloids which reach the collector surface gets attached to the surface. The ratio of particles that stick to the collector to those that strike the collector, is called the attachment efficiency, α.

Figure 2.2 represents the collision and contact mechanism of colloids with the soil grain through Brownian diffusion (D), interception (I) and gravitational sedimentation (G). Particle trajectory defines the transport path of particles, represented by solid lines, while streamlines are the lines through which groundwater flow occurs and are represented by dashed lines.

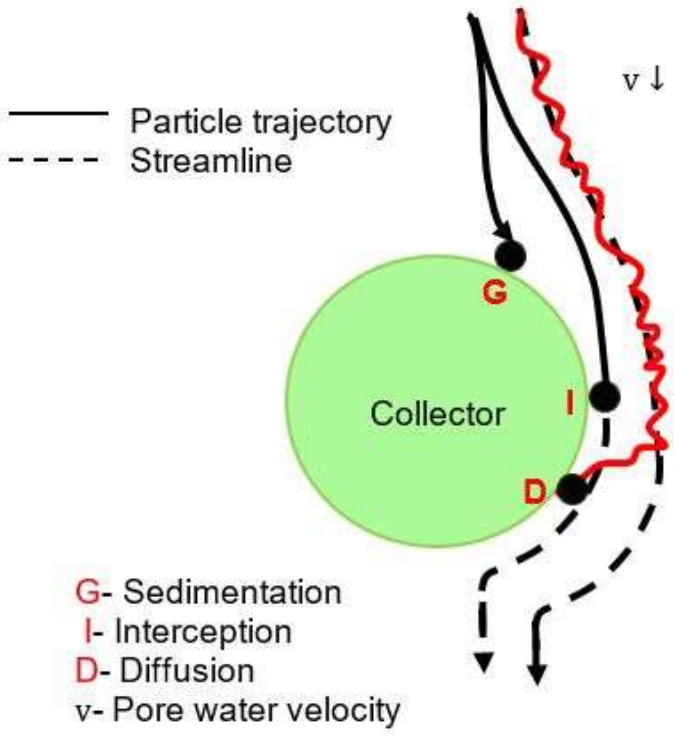

Figure 2.2 Collision and contact mechanism (Yao et al. 1971)

The collector contact efficiency, $\eta_0\ (-)$ can be defined as follows (Tufenkji and Elimelech 2004):

$$\eta_0 = \eta_D + \eta_I + \eta_G \qquad (\mathbf{2-7})$$

Eq. (2-7) can be further written as:

$$\eta_0$$

$$= 2.4\, A_S^{\frac{1}{3}} N_R^{-0.081} N_{Pe}^{-0.715} N_{vdW}^{0.052}$$

$$+ 0.55\, A_S N_R^{1.675} N_A^{0.125}, +0.22 N_R^{-0.24} N_G^{1.11}\, N_{vdW}^{0.053} \qquad (\mathbf{2-8})$$

where porosity dependant parameter $(A_S)\ (-)$ is determined from:

$$G = (1-\theta)^{1/3} \qquad (\mathbf{2-9})$$

$$A_S = \frac{2(1-G^5)}{(2-3G+3G^5-2G^6)} \qquad (\mathbf{2-10})$$

$N_R\ (-)$ is the aspect ratio and it is calculated from the ratio of nanoparticle diameter $(d_P)\ (m)$ to the collector (soil grain) diameter $(d_C)\ (m)$.

$$N_R = \frac{d_P}{d_C} \qquad (\mathbf{2-11})$$

Peclet number $(N_{Pe})(-)$ can be determined as follows:

$$N_{Pe} = \frac{v d_C}{D_B} \qquad (\mathbf{2-12})$$

where, D_B is the bulk diffusion coefficient $(m^2.s^{-1})$. Van der Wall's number $(N_{vdW})\ (-)$ is determined as follows:

$$N_{vdW} = \frac{A}{kT} \qquad (\mathbf{2-13})$$

where, A is the Hamker constant $(-)$, k is the Boltzman constant $(-)$ and T is the temperature (K). Attraction number $(N_A)(-)$ is defined as follows:

$$N_A = \frac{A}{\left(12\pi\mu_{sub} r_p^2 v\right)} \qquad (\mathbf{2-14})$$

where, μ_{sub} represents viscosity $(Pa.s)$ of the colloidal solution in the subsurface and r_P denotes the colloid radius (m). The gravity number $(N_G)(-)$ is determined as follows:

$$N_G = \frac{2r_P^2(\rho_P - \rho_F)g}{9\mu_{sub} v} \qquad (\mathbf{2-15})$$

where, g is the acceleration due to gravity $(\mathrm{m.s^{-2}})$ and ρ_F is the density of the colloidal solution $(\mathrm{kg.m^{-3}})$.

Finally, the attachment rate can be defined as:

$$k_{att} = \frac{3(1-\theta)\alpha\eta_0 \, v}{2d_C} \qquad (\mathbf{2-16})$$

and changes in attached concentration can be defined as:

$$\frac{\rho_b}{\theta}\frac{\partial S}{\partial t} = k_{att} C \qquad (\mathbf{2-17})$$

CFT can predict deposition phenomena more accurately than reversible phenomena and it accounts for traditional mechanism of filtration (Tufenkji and Elimelech 2004, Nelson and Ginn 2005). Eq. (2-18) links AD Eq. (2-1) with CFT equations to predict colloid transport in porous media:

$$\frac{\partial C}{\partial t}\theta = -q\frac{\partial C}{\partial x} + D_{Disp}\frac{\partial^2 C}{\partial x^2}\theta - \rho_b \frac{\partial S}{\partial t} \qquad (\mathbf{2-18})$$

This equation can be written with respect to concentration using Eq. (2-17):

$$\frac{\partial C}{\partial t}\theta = -q\frac{\partial C}{\partial x} + D_{Disp}\frac{\partial^2 C}{\partial x^2}\theta - \theta k_{att} C \qquad (\mathbf{2-19})$$

2.3 Darcy Law for Flow through Aquifer

Groundwater flow through a saturated aquifer is typically described by the Darcy law (De Wiest 1966):

$$\frac{\partial(\rho_F\theta)}{\partial t} + \nabla\cdot(\rho_F\vec{q}) = Q_m \qquad (\mathbf{2-20})$$

The first term $\frac{\partial(\rho_F \theta)}{\partial t}$ represents the amount of water stored in aquifer and the second term $\nabla \cdot (\rho_F \vec{q})$ refers to groundwater movement, while Q_m is the sink and source term $(kg.\, m^{-3} s^{-1})$. The Darcy velocity (q) $(m.\, s^{-1})$ is defined as follows:

$$q = -\frac{k_P \nabla P}{\mu_{sub}} \qquad (\mathbf{2-21})$$

Where, k_P is the permeability (m^2) of the aquifer porous media and ∇P is the pressure gradient $(-)$ which can be written as:

$$\nabla P = \rho_F g \nabla h \qquad (\mathbf{2-22})$$

Where, ∇h is the hydraulic gradient $(m.\, m^{-1})$ derived from the ratio of the difference in hydraulic head to the distance between two points.

2.4 Heterogeneous Porous Media

Porous media is typically modeled as homogenous using an average value of permeability for the whole domain. However, real aquifers have variable permeability distributions, as well as, layering of various soils. This means that aquifers should be modelled as heterogeneous formations with variable collector or soil grain sizes. The relationship between permeability and soil grain size is described by the Kozeny-Carman equation (Kozeny 1927, Carman 1937):

$$d_C = \sqrt{\frac{(k_P\, (1-\theta)^2 180}{\theta^3}} \qquad (\mathbf{2-23})$$

This equation can be considered for colloid transport modeling when representing heterogeneous aquifer conditions.

Chapter 3 Development of a Field-Validated Three-Dimensional Model for nZVI Subsurface Transport

In this chapter, the 3D model developed using COMSOL Multiphysics (COMSOL User's Guide 2017) is described. In particular, the modelling approach, the detailed calculations and assumptions of the model, and the comparison of the developed model with another field validated model, are described in this chapter. Portions of this chapter have been published in the Canadian Geotechnical Society (CGS) Conference (Asad et al. 2018), as such some definitions and equations are repeated from Chapter 2.

3.1 COMSOL Modeling Approach

COMSOL Multiphysics is a software platform that uses finite elements to simulate physics-based problems. It is defined as a *"Multiphysics"* platform because it can deal with various types of physical phenomena such as fluid flow, heat transfer, pore scale flow, etc. (COMSOL User's Guide 2017). Various types of physical phenomenon are built into COMSOL modules, with appropriate characteristic equations and fundamental features. These modules can be linked together, as well as, modified with additional user-defined equations (COMSOL User's Guide 2017). For this work, the Transport of Diluted Species (TDS) Module and the Darcy's Law (DL) Module were used.

3.1.1 Model Development for nZVI Transport

To model nZVI transport, and to verify and validate the 3D modelling approach, the Krol et al. (2013) study was used. Krol et al. (2013) simulated a field study (Bennett et al., 2010) in which CMC-coated nZVI was injected into a shallow granulated aquifer. Krol et al. (2013) used CompSim, a 3D finite difference, three-phase, simulator developed by Sleep and Sykes (1993), which is a proprietary software. They showed that the CompSim model was able to accurately predict the field study. Therefore, the results of the CompSim was used to verify and validate the model developed in this study to ensure that the CMC-nZVI transport was correctly implemented using COMSOL, a commercially available software.

3.1.2 Numerical Approach

The DL module defines Darcy's law in COMSOL by:

$$\frac{\partial(\rho_F \theta)}{\partial t} + \nabla.(\rho_F q) = Q_m \qquad (\mathbf{3-1})$$

Where q is the Darcy velocity $(m.s^{-1})$, θ is the porosity $(-)$, and ρ_F is the fluid density $(kg.m^{-3})$. A 3D Darcy velocity field is created in the DL module which is transferred to the TDS module, where the transport of polymer coated nanoparticles in a porous media is described by Eq (3-2) which is the 3D version of Eq. (2-19):

$$\frac{\partial C}{\partial t}\theta = -q\frac{\partial C}{\partial x} - q\frac{\partial C}{\partial y} - q\frac{\partial C}{\partial z} + D_{Disp}\frac{\partial^2 C}{\partial x^2}\theta + D_{Disp}\frac{\partial^2 C}{\partial y^2}\theta + D_{Disp}\frac{\partial^2 C}{\partial z^2}\theta - \theta k_{att} C \qquad (\mathbf{3-2})$$

Where C is the aqueous nZVI concentration $(\mathrm{mol.\,m^{-3}})$ at a distance of x (m) and time $\mathrm{t}\,(\mathrm{s})$, q is the Darcy velocity $(\mathrm{m.\,s^{-1}})$ ($\mathrm{q} = \theta \mathrm{v}$ where v is the porewater velocity$(\mathrm{m.\,s^{-1}})$). $\mathrm{D_{disp}}$ is the effective hydrodynamic dispersion tensor $(\mathrm{m^2.\,s^{-1}})$.

Attachment rate coefficient $\mathrm{k_{att}}$ $(\mathrm{s^{-1}})$ is defined by the CFT (Tufenkji and Elimelech 2004) and expressed as:

$$\mathrm{k_{att}} = \frac{3(1-\theta)\alpha\eta_0 \mathrm{v}}{2\mathrm{d_C}} \qquad (\mathbf{3-3})$$

Where α is the attachment efficiency $(-)$, η_0 is the collector contact efficiency $(-)$, $\mathrm{d_C}$ is the collector (soil grain) diameter (m). It is to be noted that the term $\mathrm{k_{att}}$ $(\mathrm{s^{-1}})$ is applied for nZVI transport only. The polymer (CMC) is considered a conservative species, and therefore the attachment rate for the polymer is zero.

3.1.3 Conceptual Model

Figure 3.1 shows a conceptual model of an injection well in the middle of a 3D domain that injects polymer (CMC) coated nZVI into an aquifer with groundwater flowing from left to right. This conceptual model has been implemented in COMSOL.

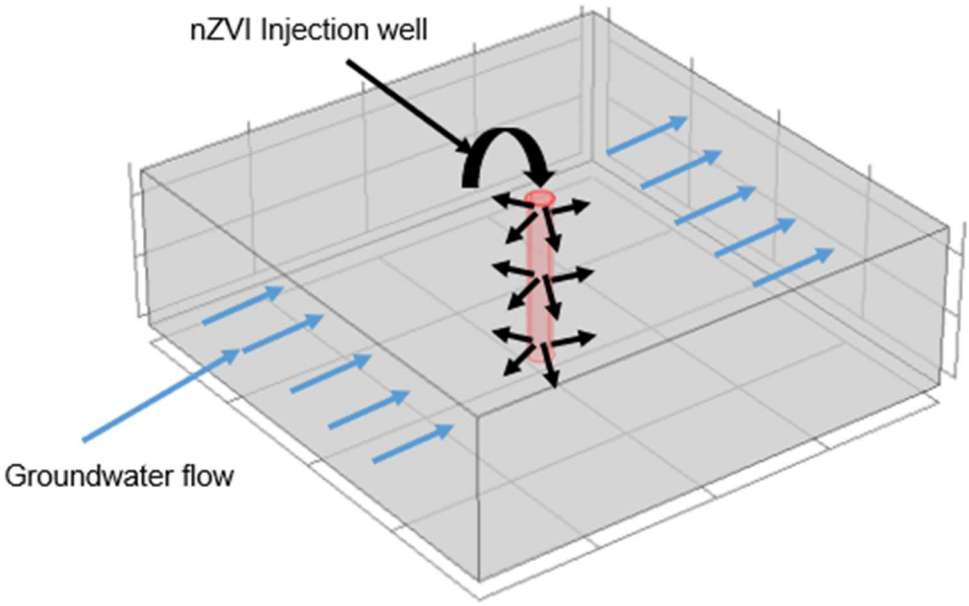

Figure 3.1: Model schematic

3.1.4 Boundary Conditions

Figure 3.2 shows the boundary conditions (BC) and characteristics of half of the 3D domain since a symmetrical BC has been used along the XZ plane (through the injection well) to split the domain into half and minimize computational time. The model represents a remediation scenario, therefore a cylindrical injection well has been defined in the middle of the domain which injects a CMC-coated nZVI solution into the subsurface. The initial solution concentration is defined as zero in the domain and the direction of groundwater flow is from left to right defined by the *constant hydraulic head* BC.

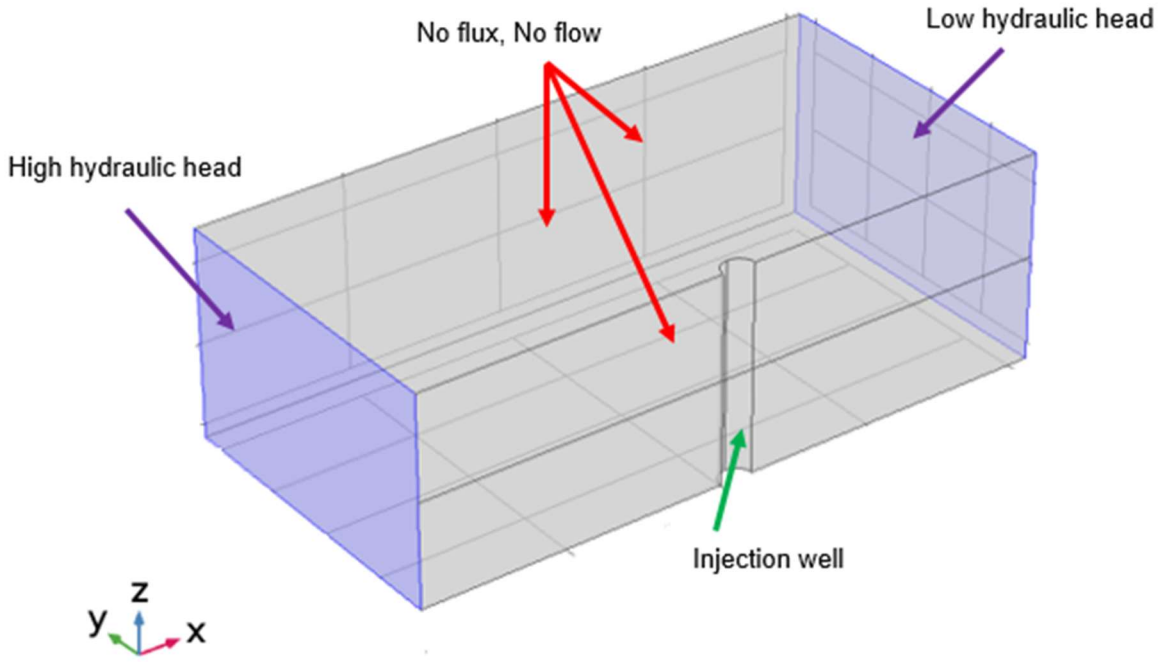

Figure 3.2: Boundary conditions for half of a 3D domain

No flow and *no flux* BC have been defined at the upper, lower, and side boundaries. The injection well can be used for defining a water mass flow rate $(\mathrm{m}^3.\mathrm{s}^{-1})$ in the DL module and a nZVI and polymer constant flux $(\mathrm{mol}.\mathrm{m}^{-2}.\mathrm{s}^{-1})$ in the TDS module.

3.1.5 Parameters and Variables

To simulate the Krol et al (2013) domain, the same parameters were used and are summarized in Table 3.1. These parameters represent the properties of the subsurface domain, nZVI and polymer characteristics, and necessary constants and variables.

Table 3.1 Basic simulation parameters (adapted from Krol et al (2013))

Name	Symbol	Value
Length of domain	L	4 (m)
Radius of injection well	R_I	0.05 (m)
Density of porous media	ρ_b	1250 $(kg.m^{-3})$
Porosity	θ	0.36 $(-)$
Average density of nZVI solution	ρ_F	1000 $(kg.m^{-3})$
nZVI diameter	d_P	1.40x10^{-7} (m)
Collector diameter	d_C	2x10^{-4} (m)
Hamaker constant	A	3x10^{-21} (J)
Boltzmann constant	k	1.4x10^{-23} $(J.k^{-1})$
Temperature	T	293 (K)
Diffusion coefficient (nZVI)	D_{FN}	3x10^{-9} $(m^2.s^{-1})$
Diffusion coefficient (polymer)	D_{FP}	1x10^{-9} $(m^2.s^{-1})$
Permeability	k_P	3.6x10^{-11} (m^2)
Hydraulic gradient	∇h	0.0142 $(m.m^{-1})$
Attachment efficiency	α	0.02 $(-)$
CMC molecular weight	M_{WP}	90 $(kg.mol^{-1})$
CMC percentage	P_t	0.8 $(\%)$
nZVI injection concentration	C_I	0.96 $(kg.m^{-3})$

3.1.6 Parameters from Colloid Filtration Theory

To simulate the transport of CMC coated nZVI, the transport equation (Eq. 2-1) was modified with the CFT equation. Single collector contact efficiency (η_0), a variable in the CFT equation requires calculation of several parameters. While some values are fixed at the start of a model, other values vary with time and space, for example porewater velocity, producing a non-linear system which is sensitive to initial conditions and can result in numerical convergence challenges.

Single collector contact efficiency (η_0) can be determined as follows (Tufenkji and Elimelech 2004):

$$\eta_0 = 2.4\, A_S^{1/3} N_R^{-0.081} N_{Pe}^{-0.715} N_{vdW}^{0.052} + 0.55\, A_S N_R^{1.675} N_A^{0.125} + 0.22 N_R^{-0.24} N_G^{1.11}\, N_{vdW}^{0.053} \quad (\mathbf{3-4})$$

where, A_S is called the porosity dependent parameter $(-)$, N_R is the aspect ratio $(-)$, N_{Pe} is the Peclet number $(-)$, N_{vdW} is the Van der Wall's number $(-)$, N_A is the attraction number $(-)$ and N_G is the gravity number $(-)$. $A_S(-)$, N_{vdW} $(-)$ and N_R $(-)$ are fixed parameters. N_{Pe} $(-)$ depends on both porewater velocity $(v)(m.s^{-1})$ and bulk diffusion coefficient $(D_B)(m^2.s^{-1})$. Both N_A and N_G depend on porewater velocity $(v)(m.s^{-1})$ and subsurface viscosity$(\mu_{sub})(Pa.s)$, which is the dynamic viscosity of injected CMC coated nZVI solution. All variables are defined in Chapter 2.

3.2 Calculation of Mole Fraction, Subsurface Viscosity and Modeling Well Injection

Similarly to Krol et al (2013), the injected solution consisted of 0.8% of 90 (kg/mol) CMC polymer and 0.96 g/L nZVI. The specific values used in COMSOL are outlined in this section.

3.2.1 nZVI and Polymer Mole Fractions

COMSOL solves two dependent variables for the aqueous concentrations of nZVI and polymer, (C_N) $(mol.m^{-3})$ and (C_P) $(mol.m^{-3})$ respectively. In COMSOL, the unit $(mol.m^{-3})$ represents the moles of species per unit of total volume. However,

typically field nZVI injections are given in terms of mole fractions(X_N and X_P) therefore the concentrations are related as follows:

$$X_N = \left(\frac{C_N\, x_{ni}}{\theta\, C_{in}}\right) \qquad (\mathbf{3-5})$$

$$X_P = \left(\frac{C_P\, x_{pi}}{\theta\, C_{ip}}\right) \qquad (\mathbf{3-6})$$

where x_{ni} $(\frac{\text{mol of nZVI}}{\text{mol of water}})$ and x_{pi} $(\frac{\text{mol of polymer}}{\text{mol of water}})$ are the initial mole fractions of nZVI, and polymer respectively and C_{in} (mol.m^{-3}) and $C_{ip}(\text{mol.m}^{-3})$ are initial molar concentration of nZVI and polymer respectively. θ is soil porosity $(-)$ (to convert from total volume to water volume). The mole fractions vary in each node of the model as concentration varies with time.

3.2.2 Initial nZVI Mole Fractions

Initial mole fraction of nZVI (x_{ni}) $(\frac{\text{mol of nZVI}}{\text{mol of water}})$ is measured as follows:

$$X_{in} = \frac{(\frac{\text{nZVI Concentration } (\frac{\text{kg}}{\text{m}^3})}{\text{molecular weight of nZVI } (\frac{\text{kg}}{\text{mol}})})}{\text{molecular weight of water } (\frac{\text{mol of water}}{\text{m}^3\text{of water}})} = \frac{(\frac{0.96\ (\frac{\text{kg of nZVI}}{\text{m}^3\text{ of water}})}{0.0558\ (\frac{\text{kg of nZVI}}{\text{mol of nZVI}})})}{55450\ (\frac{\text{mol of water}}{\text{m}^3\text{of water}})}$$

$$= 3.10 * 10^{-4}\ \frac{\text{mol of nZVI}}{\text{mol of water}} \qquad (\mathbf{3-7})$$

3.2.3 Initial Polymer Mole Fractions

To determine initial mole fraction of CMC polymer in water, moles of polymer with respect to the total solution weight of 100 kg was calculated:

$$\text{Moles of polymer} = \frac{0.8\ \frac{\text{kg of polymer}}{\text{total kg}}}{\text{molecular weight of polymer}\ (\frac{\text{kg of polymer}}{\text{mol of polymer}})} = \frac{0.8}{90}$$

$$= 8.88 * 10^{-3}\ \frac{\text{mol of polymer}}{\text{total kg}} \qquad (\mathbf{3-8})$$

Then moles of water with respect to total weight was calculated.

$$\text{Moles of water} = \frac{(100-0.8)\ \frac{\text{kg of water}}{\text{total kg}}}{\text{molecular weight of water}(\frac{\text{kg of water}}{\text{mol of water}})} = \frac{99.2}{0.018}$$

$$= 5511\ \frac{\text{mol of water}}{\text{total kg}} \qquad (\mathbf{3-9})$$

Finally, initial mole fraction $(\mathrm{x_{pi}})$ $(\frac{\text{mol of polymer}}{\text{mol of water}})$ of CMC polymer in water is calculated by dividing molality by moles of water in total weight.

$$\mathrm{x_{pi}} = \frac{\text{mol of polymer}\ (\frac{\text{mol of poly}}{\text{total kg}})}{\text{mol of water}\ (\frac{\text{mol of water}}{\text{total kg}})} = \frac{8.88 * 10^{-3}}{5511}$$

$$= 1.615 * 10^{-6}\ \frac{\text{mol of polymer}}{\text{mol of water}} \qquad (\mathbf{3-10})$$

3.2.4 Subsurface Viscosity

When the CMC-nZVI solution is injected into the subsurface, the subsurface viscosity is calculated at every node since the mole fraction of nZVI and polymer (i.e., $\mathrm{X_N}$ $(\frac{\text{mol of nZVI}}{\text{mol of water}})$ and $\mathrm{X_P}$ $(\frac{\text{mol of polymer}}{\text{mol of water}})$) changes. The equation for calculating subsurface viscosity $(\mu_{sub})(\mathrm{Pa.s})$ of the solution is:

$$\mu_{sub} = 10^{\mathrm{X_P}\log(\mu_p) + \mathrm{X_N}\log(\mu_{nf}) + \mathrm{x_w}\log(\mu_{wf})} \qquad (\mathbf{3-11})$$

This equation uses the X_N and X_P in each node and varies the subsurface viscosity accordingly.

3.2.5 Calculation of Unknown Polymer Viscosity

Polymer viscosity is difficult to determine from experiments as it varies in a diluted solution due to its dependence on solution concentration (Budtov 1967, Dill 1980). To calculate the viscosity of the injected solution the Grunberg and Nissan equation was used (Grunberg and Nissan 1949) :

$$\log(\mu_{sol}) = x_{pi} \log(\mu_p) + x_{ni} \log(\mu_{nf}) + x_w \log(\mu_{wf}) \qquad (\mathbf{3-12})$$

Where μ_{sol} is the solution viscosity $(\mathrm{Pa.s})$ determined from experiments. For the stated amount of polymer and nZVI injection, the solution viscosity $(\mu_{sol})(\mathrm{Pa.s})$ is found to be 0.013 $(\mathrm{Pa.s})$ (Krol et al. 2013), while the nZVI viscosity is taken to be that of water which is 0.001 $(\mathrm{Pa.s})$ as nanoparticle viscosity is found to be very close to this value (Mishra et al. 2014). Since the initial mole fraction nZVI (x_{ni}), initial mole fraction CMC polymer (x_{pi}), and viscosity of nZVI $(\mu_{nf})(\mathrm{Pa.s})$ and water $(\mu_{wf})(\mathrm{Pa.s})$ are known, the polymer viscosity $(\mu_p)(\mathrm{Pa.s})$ is determined using Eq. (3-12) as follows:

$$\log(\mu_p) = \frac{\log(\mu_{sol}) - x_{ni} \log(\mu_{nf}) - x_w \log(\mu_{wf})}{x_{pi}} \qquad (\mathbf{3-13})$$

$$\log(\mu_p) = \frac{\log(0.013) - 3.10 * 10^{-4} * \log(0.001) - 1 * \log(0.001)}{1.165 * 10^{-6}} \qquad (\mathbf{3-14})$$

$$\log(\mu_p) = 6.9033 * 10^5 \qquad (\mathbf{3-15})$$

This value is then used in Eq. (3-11) to calculate the subsurface viscosity $(\mu_{sub})(\mathrm{Pa.s})$ at different nodes with time.

3.2.6 Modeling Well Injection in COMSOL

In the DL module, a mass flux boundary was defined using an injection rate. If $\mathrm{I_R}$ is the solution injection rate $(\mathrm{m^3.s^{-1}})$, $\mathrm{R_I}$ is the injection well radius (m) and $\mathrm{H_I}$ is the height of injection well (m) (i.e., Figure 3.2); the mass flux $(\mathrm{M_F})$ $(\mathrm{kg.m^{-2}.s^{-1}})$ can be determined as follows:

$$\mathrm{M_F} = \frac{\mathrm{I_R}\rho_\mathrm{F}}{\pi \mathrm{R_I H_I}} \qquad (\mathbf{3-16})$$

The mass flux $(\mathrm{M_F})$ $(\mathrm{kg.m^{-2}.s^{-1}})$ is related to the flow into the domain

$$\mathrm{M_F} = \mathbf{n}.\rho_\mathrm{F} q \qquad (\mathbf{3-17})$$

Where $\mathbf{n}$ is a vector normal to the boundary. A positive value of the mass flux indicates injection into the system and a negative value indicates an extraction. In this modeling case, inward flux has been defined.

In TDS module, a flux boundary can be defined which takes the nZVI flux and polymer flux values separately. The nZVI flux $(\mathrm{F_N})(\mathrm{mol.m^{-2}.s^{-1}})$ is defined as follows:

$$\mathrm{F_N} = \frac{\mathrm{C_I I_R}}{\pi \mathrm{R_I H_I M_{WN}}} \qquad (\mathbf{3-18})$$

where $\mathrm{C_I}$ is the nZVI injection concentration $(\mathrm{kg.m^{-3}})$, $\mathrm{I_R}$ is the injection rate $(\mathrm{m^3.s^{-1}})$, $\mathrm{M_{WN}}$ is the molecular weight of nZVI $(\mathrm{kg.mol^{-1}})$. The relation of this nZVI flux $(\mathrm{F_N})$ to advection and dispersion terms of Eq. (3-2) is as follows:

$$F_N = \mathbf{n}.(-qC + D_{Disp}\nabla C) \qquad (\mathbf{3-19})$$

Where $\mathbf{n}$ is a vector normal to the boundary. A positive value of the nZVI flux (F_N) $(\mathrm{mol.\,m^{-2}.\,s^{-1}})$ indicates inward flux in the system and a negative value indicates an outward flux. In this modeling case, inward flux has been defined.

Similarly, the polymer flux (F_P), was defined as follows:

$$F_P = \frac{C_P I_R}{\pi R_I H_I M_{WP}} \qquad (\mathbf{3-20})$$

If C_P is the polymer injection concentration $(\mathrm{kg.\,m^{-3}})$, I_R is the injection rate $(\mathrm{m^3.\,s^{-1}})$, M_{WP} is the molecular weight of polymer $(\mathrm{kg.\,mol^{-1}})$

And the relation between polymer flux (F_P) $(\mathrm{mol.\,m^{-2}.\,s^{-1}})$ with advection and dispersion terms of Eq. (3-2) is following

$$F_P = \mathbf{n}.(-qC + D_{Disp}\nabla C) \qquad (\mathbf{3-21})$$

Where $\mathbf{n}$ is a vector normal to the boundary.

3.3 Verification of Model Results

The COMSOL model was verified using the Krol et al. (2013) study. Figures 3.3 and 3.4 compare relative nZVI concentration $(\frac{C}{C_0})$ and subsurface viscosity $(\mu_{sub})(\mathrm{Pa.\,s})$ of the COMSOL and CompSim models respectively after 1 and 20 hours of constant injection.

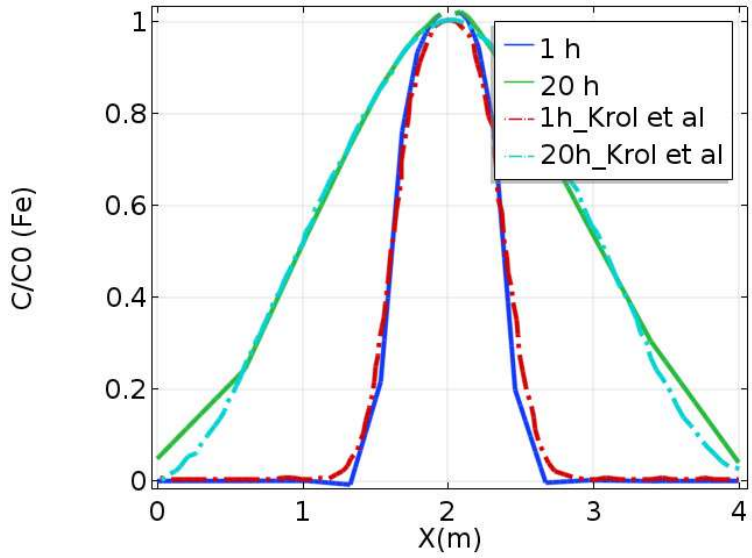

Figure 3.3: Comparison of COMSOL and CompSim (Krol et al. 2013) concentrations

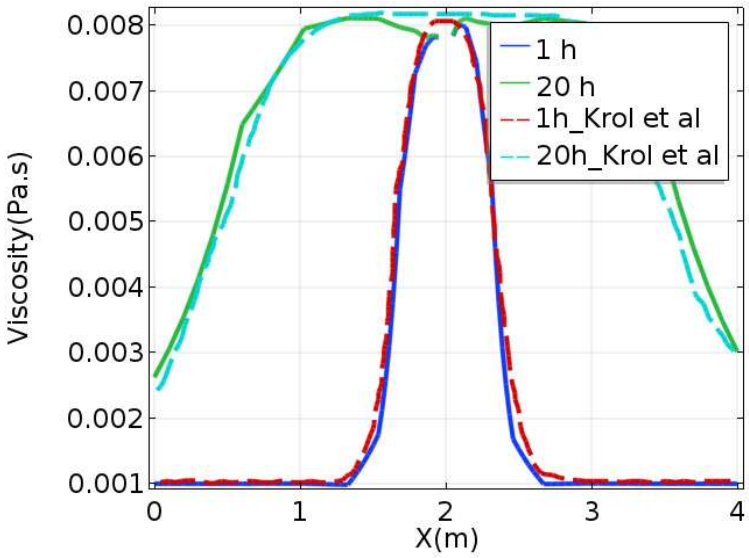

Figure 3.4: Comparison of COMSOL and CompSim (Krol et al. 2013) viscosity

Figures 3.3 and 3.4 show a similar distribution of relative nZVI concentration $(\frac{C}{C_0})$ and subsurface viscosity (μ_{sub}) for both COMSOL and CompSim models. In

addition to this qualitative comparison, the difference between the values of the distribution was calculated using the following general formula:

$$\text{Difference} = \sqrt{\frac{\sum_{j=1}^{J}(Y_{COMSOL} - Y_{CompSim})^2}{J}} \qquad (\mathbf{3-22})$$

Where J is the number of observations. Table 3.2 shows the difference between COMSOL and CompSim simulation outcome considering values corresponding to Figure 3.3 and Figure 3.4.

Table 3.2: Difference between COMSOL and CompSim model results

Time	$C/C_0\,(-)$	$\mu_{sub}(\mathbf{Pa.s})$
1 hour	0.035	0.00025
20 hours	0.021	0.00026

Table 3.2 shows that the difference is very low indicating good agreement between the two model results. To rule out mesh dependence, the simulation was performed for various mesh size (i.e., coarse to extra fine mesh). Figure 3.5 compares nZVI concentration plots for three different mesh sizes, using identical input for all three simulations. Negligible difference can be seen among three concentration plots but the finer mesh simulation resulted in a smoother concentration profile due to more elements of smaller size. For the rest of the simulations a fine mesh was used.

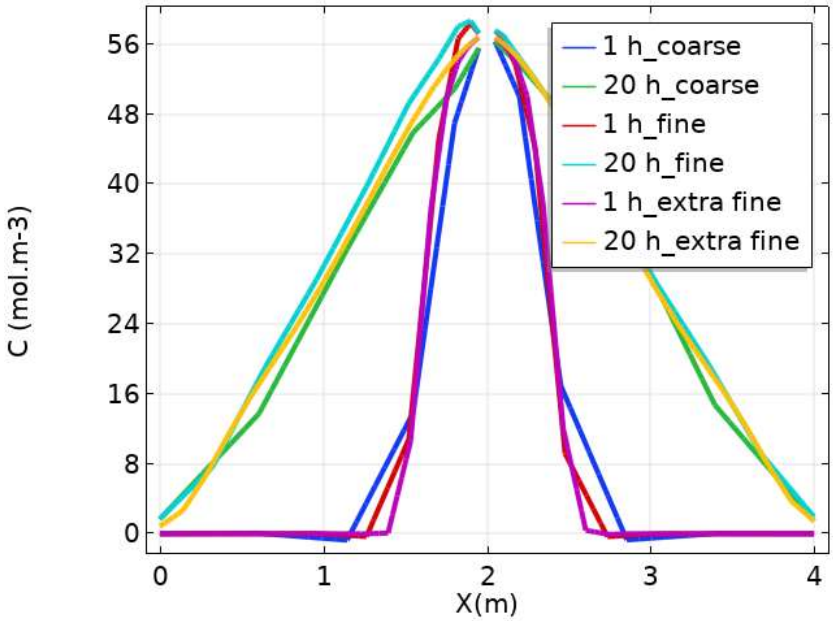

Figure 3.5: Comparison of COMSOL concentration plots for varying mesh size

3.4 3D nZVI Transport in Porous Media

nZVI injection into the subsurface is typically performed using an injection well. To better depict and predict remediation scenarios and to study the effect of various factors, a 3D model is needed. Figure 3.5 represents a simulated 3D domain showing nZVI spread from a constant flux injection well after 20 hours of injection into a homogeneous domain.

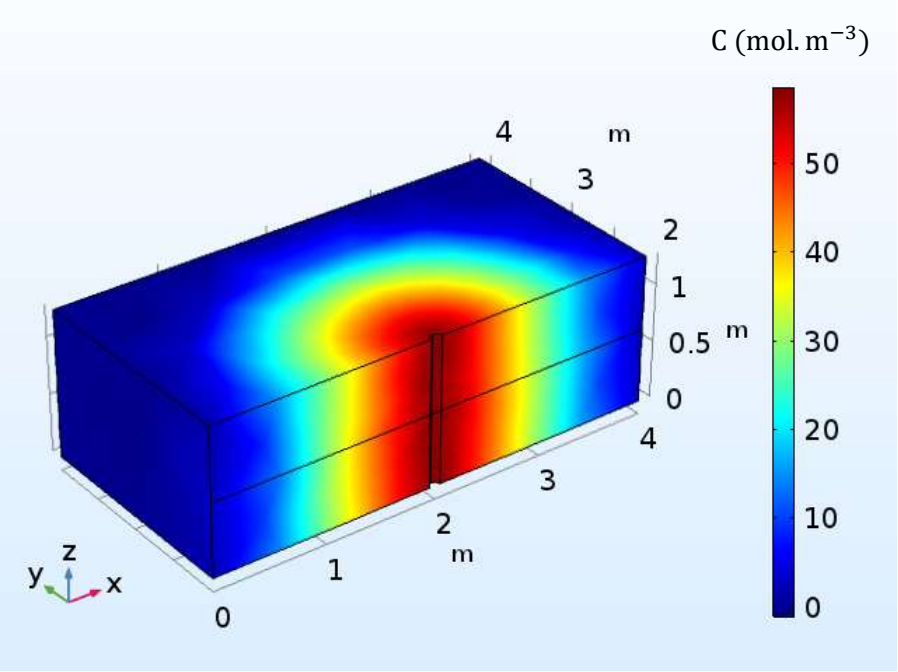

Figure 3.6: nZVI spread after 20 hours of injection

3.5 Conclusions

In this chapter, a detailed procedure for a 3D homogeneous nZVI transport model development in COMSOL was described. The developed model followed the approach of Krol et al. (2013), who simulated and validated a field injection of CMC-coated nZVI (Bennet et al. (2010). Detailed numerical approach, boundary conditions, parameter selection, calculation of mole fractions, viscosity and flux have been documented. Verification of model results was done by comparing both model concentration and viscosities to the simulated results of Krol et al. (2013). The very low difference between the two model results was found indicating good agreement between the two studies.

Chapter 4 Development of a Heterogeneous Two-Dimensional nZVI Transport Model

Subsurface heterogeneity can affect nZVI travel distance by hindering nZVI transport, diverting nZVI flow from desired direction (i.e., preferential flow), and transporting injected nZVI solution to the surface (i.e., daylighting of solution) during field injection (Henn and Waddill 2006, Su et al. 2013, Kocur et al. 2014) . In addition, phenomena such as aggregation and straining are greatly influenced by soil particle size which varies with variable permeability distribution. As natural aquifers are heterogeneous in nature, modeling studies should incorporate heterogeneity to investigate its effect and optimize nZVI technology. There are few studies (Cullen et al. 2010, Strutz et al. 2016, Mondal et al. 2018) which considered nZVI distribution in a heterogeneous domain. Although these studies have investigated the role of heterogeneity and sensitivity of some factors on nanoparticles and nZVI transport through experiments and simulations, no studies have investigated the statistically significant impact of possible factors on nZVI transport in heterogeneous aquifers representing field aquifer conditions.

In this chapter, the validated model from Chapter 3 was used to simulate a 2D heterogeneous domain. The numerical approach, boundary conditions, parameters and variables, permeability distribution realizations, and the effect of subsurface heterogeneity are discussed below.

4.1 2D Heterogeneous COMSOL Model

The development of a 2D heterogeneous model in COMSOL is similar to that of the field validated 3D model described in Chapter 3. While the calculation procedure for time and space dependant mole fractions, subsurface viscosity, and molar flux are as same as the 3D model, there is an additional equation that links the heterogeneous permeability field to the CFT equation. The Kozeny-Carman equation, (Kozeny 1927, Carman 1937, 1956) describes the relationship between the collector diameter $\mathrm{d_C(m)}$ and the soil permeability $\mathrm{k_P(m^2)}$.

$$\mathrm{d_C} = \sqrt{\frac{\mathrm{k_P}\ (1-\theta)^2 180}{\theta^3}} \qquad (\mathbf{4-1})$$

It is to be noted that this equation is only valid for laminar flow.

4.1.1 Boundary Conditions for 2D Model

Figure 4.1 represents the BC and characteristics of a full 2D domain. An injection well was defined in the middle of the domain which injects the CMC-coated nZVI solution into the subsurface, representing a vertical soil profile of the subsurface. The initial CMC-nZVI concentration is defined as zero in the domain. The direction of groundwater flow is defined from left to right due to the *"constant hydraulic head"* BC, while the *"no flow"* and *"no flux*" BCs have been defined at the upper and lower boundaries.

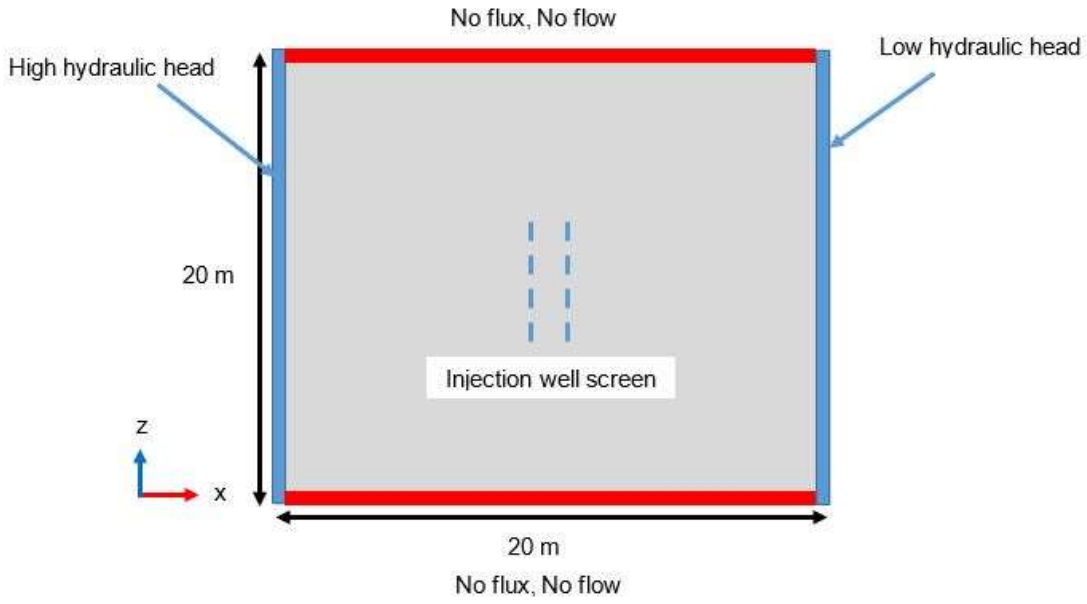

Figure 4.1 : Boundary conditions for a full 2D domain, representing a vertical cross-section

4.1.2 Parameters and Variables for 2D Model

In the 2D model, a 20m x 20m vertical soil profile was simulated in COMSOL. While most of the simulation parameters are the same as the Krol et al (2013) homogenous domain (Table 3.1), the collector diameter is variable for this 2D model because permeability varies in a heterogeneous medium.

To simulate the transport of CMC coated nZVI in a 2D heterogeneous aquifer, the 2D transport equation was used.

$$\frac{\partial C}{\partial t}\theta = -q\frac{\partial C}{\partial x} - q\frac{\partial C}{\partial z} + D_{Disp}.\frac{\partial^2 C}{\partial x^2}\theta + D_{Disp}.\frac{\partial^2 C}{\partial z^2}\theta - \theta k_{att} C \qquad (\mathbf{4-2})$$

The parameters and variables associated with single collector contact efficiency (η_0) equation (Eq. 3-4) were examined in light of the added heterogeneity. $\mathrm{A_S}(-)$ and $\mathrm{N_{vdW}}(-)$ are fixed parameters for the 2D heterogeneous model, but, $\mathrm{N_R}(-)$ and $\mathrm{N_{Pe}}(-)$, fixed parameters in 3D model, become variable in this 2D model due to change in collector diameter (calculated by Eq. 4-1). This is due to the variable permeability distribution in the vertical soil profile. $\mathrm{N_A}(-)$ and $\mathrm{N_G}(-)$ remain variable in 2D as they were in the 3D model, due to their dependence on porewater velocity (Eq. 2-14 and Eq. 2-15).

4.2 nZVI Distribution in Heterogeneous Subsurface

To examine the effect of subsurface heterogeneity on nZVI transport, one hundred permeability realizations for two aquifers with different heterogeneities (i.e., Borden and Swiss) were generated using the Field Generator in PMWIN (Processing Modflow 5.3) which uses Mejia's algorithm (Mejía and Rodríguez-Iturbe 1974, Frenzel 1995). This algorithm works by determining the covariance of the randomly distributed data field. Covariance considers multiplication of standard deviations (for both independent and dependent variable) and correlation function which characterizes the data field (Snedecor and Cochran 1980, Spiegel 1992). In this scenario, permeability is the dependent variable and length of the aquifer is the independent variable. Using the algorithm, the Field Generator (Processing Modflow 5.3) takes basic characteristics (i.e., mean, the variance of permeability

distribution and correlation length) of aquifers which are well documented in the literature (Table 4.1). Mean and variance of permeability distribution provide the Generator information about the permeability of aquifer, while the correlation length defines the maximum distance after which deviation between dependent variable (i.e., permeability) and the mean becomes different, and an estimation of randomness (Bhushan 2000). In this context, correlation length provides an idea about the size of the permeability variation with aquifer length.

The mean permeability, correlation length, and porosity are same for both aquifers, but the Swiss aquifer has a higher variance in permeability resulting in greater contrast in permeability fields (Table 4.1). Therefore, the Swiss aquifer is considered more heterogeneous than the Borden aquifer. It is to be noted that the permeability distribution was taken into COMSOL by an “Interpolation” function. This function takes permeability distribution data directly as input and does not change the discretization. This means that the data is placed in the same location on a 20m x 20m domain, as they were located on the Field Generator.

4.2.1 Aquifers of Various Heterogeneity

The Borden aquifer was chosen for this study as it is relatively homogeneous and well characterized (Sudicky 1986, Dekker and Abriola 2000). The Swiss aquifer was chosen as it is more heterogeneous compared to Borden aquifer due to a higher variance in permeability (Jussel et al. 1994, Dekker and Abriola 2000). This higher variance in permeability results in a higher contrast in permeability as

compared to the Borden aquifer and allows for a comparison of the effect of permeability on nZVI transport. Table 4.1 represents aquifer properties and simulation parameters for the initial simulations (Base Case) in a 2D heterogeneous domain.

Table 4.1: Aquifer properties and simulation parameters for two heterogeneous aquifers

Name (unit)	Symbol	Value	
		Borden aquifer	**Swiss aquifer**
Porosity $(-)^{a}$	θ	0.34	0.34
Average permeability $(\mathrm{m}^2)^{b,c}$	$\mathrm{k_P}$	1.1×10^{-11}	1.6×10^{-11}
Variance $(\log(\mathrm{k}_P))\ (-)^{b,c}$	σ	0.2130	0.4343
Mean $(\log(\mathrm{k}_P))\ (-)^{b,c}$	μ	-11.01	-11.01
Average diameter of collector (m)	$\mathrm{d_C}$	1.50×10^{-4}	1.75×10^{-4}
Horizontal correlation length $(\mathrm{m})^{b}$	$\mathrm{x_h}$	5.1	5.1
Vertical correlation length $(\mathrm{m})^{b}$	$\mathrm{z_v}$	0.21	0.21
Anisotropy factor $(-)^{d}$	$\mathrm{A_F}$	0.5	0.5
nZVI injection concentration $(\mathrm{kg.\,m^{-3}})^{e}$	$\mathrm{C_I}$	0.96	0.96
Base Case porewater velocity $(\mathrm{m.\,day^{-1}})^{e}$	v	0.1	0.1
Base Case nZVI flux $(\mathrm{mol.\,m^{-2}.\,s^{-1}})^{e}$	$\mathrm{F_N}$	0.009	0.009
Base Case injection viscosity $(\mathrm{Pa.\,s})^{e}$	μ_{sub}	0.013	0.013

Sources: ([a]Sudicky 1986, [b]Woodbury and Sudicky 1991, [d]Brown et al. 1994, [c]Jussel et al. 1994, [e]Krol et al. 2013)

4.2.2 Selection of Number of Realizations for Permeability Distribution

The estimate of variance of the nZVI center of mass at 24 hours was calculated for randomly selected permeability realizations. It was found that convergence of variance occurred within 15 realizations (Figure 4.2), therefore 15 permeability

realizations (out of 100) were chosen for both aquifers (Borden or Swiss) at random to perform the analysis. This means that 15 realizations are representative of the aquifer variability while optimizing simulation time.

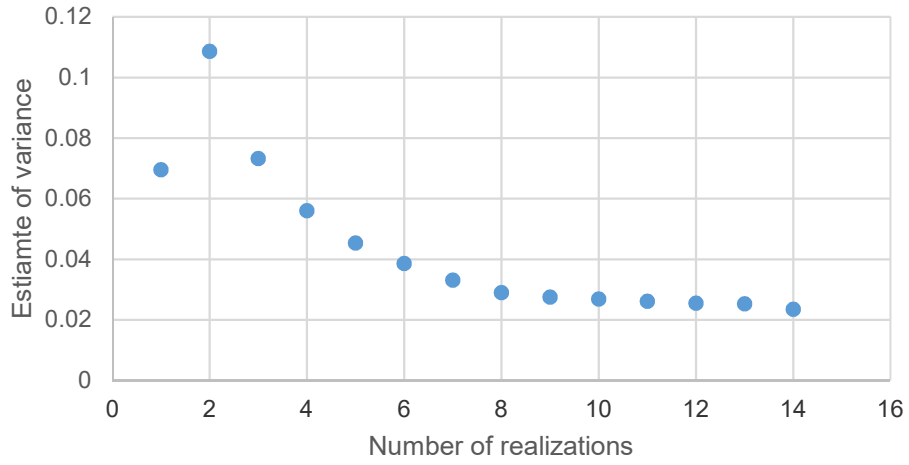

Figure 4.2: Estimate of variance for center of mass of Borden aquifer

4.2.3 Effect of Soil Heterogeneity on nZVI Transport

Figure 4.3 shows the permeability distribution of the Borden and Swiss aquifers for one of the realizations. These two realizations are generated by the Field Generator and have a difference in permeability variance only (nZVI injection flux and other simulation parameters are identical).

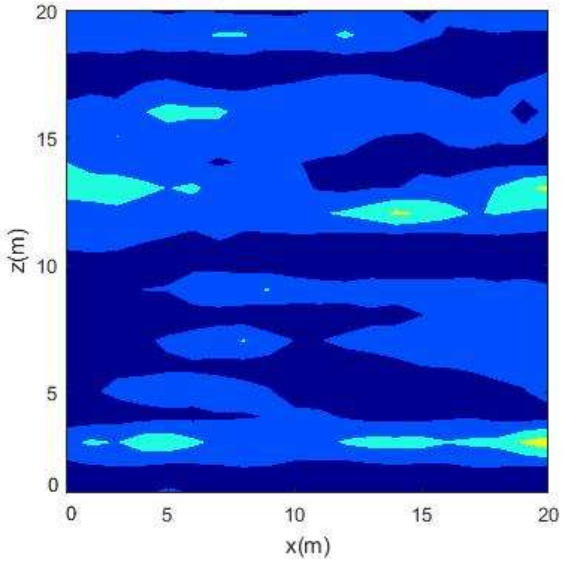

(a) Borden Aquifer

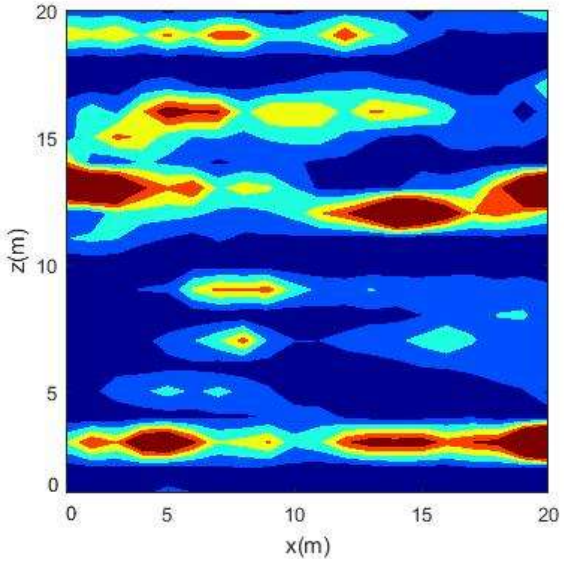

(b) Swiss Aquifer

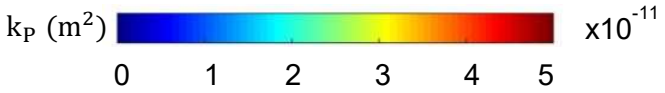

Figure 4.3: Aquifer permeability distribution for (a) Borden aquifer (b) Swiss aquifer

Figure 4.3 shows that greater variation in permeability is observed in the

Swiss aquifer than in the Borden aquifer, while Figure 4.4 shows the nZVI distribution for the two aquifers (with the permeability shown in Figure 4.3).

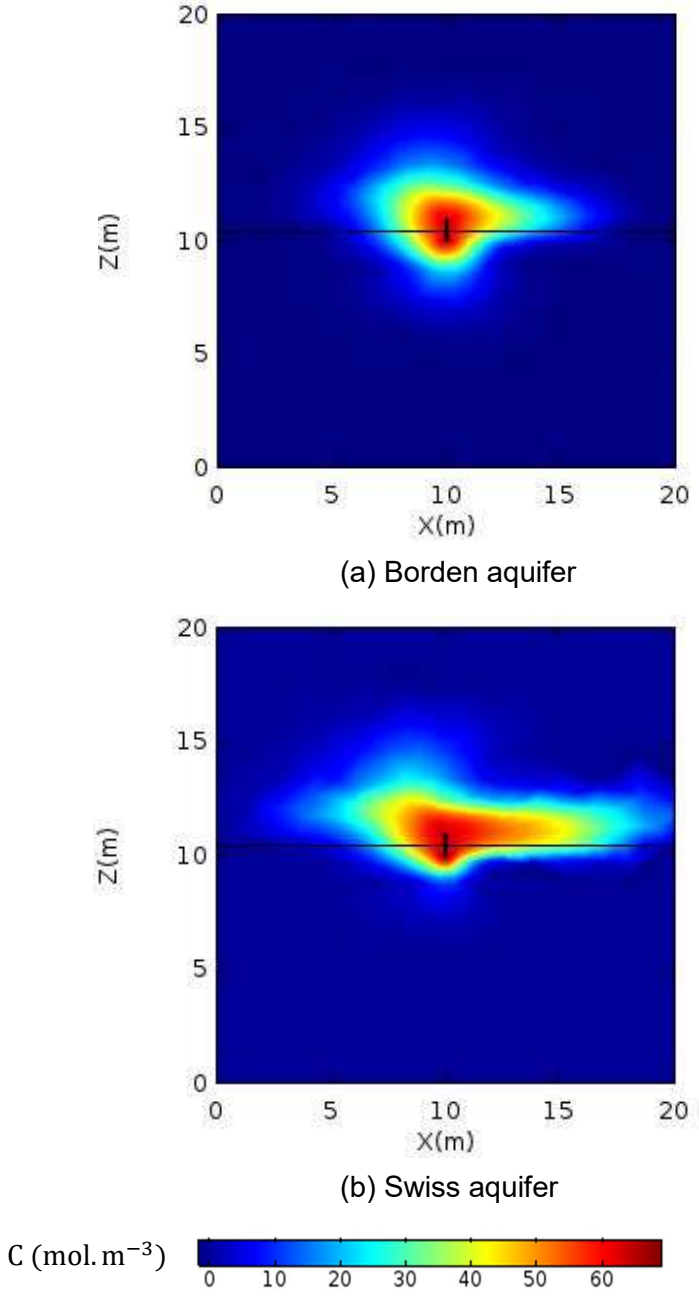

Figure 4.4: Aqueous nZVI distribution in (a) Borden aquifer (b) Swiss aquifer at 48 hours

nZVI movement in the Borden aquifer (Figure 4.4a) seems to be confined around the injection well while nZVI appears to be more dispersed in the Swiss aquifer (Figure 4.4b). This dispersed movement is due to the aquifer heterogeneity with nZVI following a preferential flow path as outlined by the high permeability zone seen in Figure 4.3b.

Similarly, Figure 4.5 shows nZVI distribution in both aquifers for three different permeability realizations after 48 hours of injection., while keeping all other simulation parameters the same. It can be seen from Figure 4.5 that while Borden aquifer realizations show a nearly circular nZVI distribution around the well, Swiss aquifer realizations exhibit a more dispersed pattern due to the higher variance of soil permeability. Similarly to Figure 4.4b, nZVI in the Swiss aquifer follows the high permeability zones leading to more lateral spreading. These results show that nZVI distribution is likely to be impacted by subsurface heterogeneity.

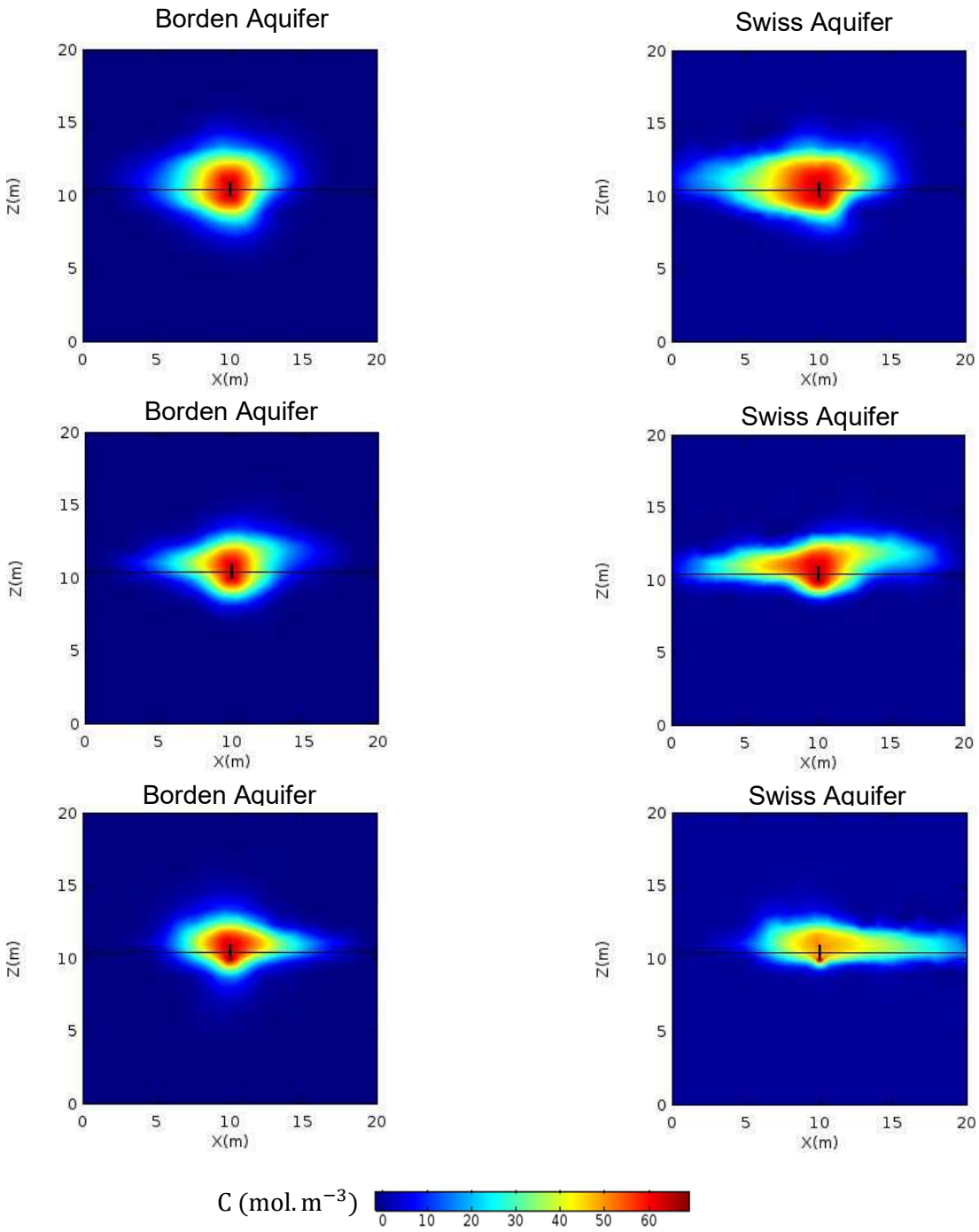

Figure 4.5: nZVI distribution in Borden and Swiss aquifer for three different permeability realizations at 48 hours.

4.3 Conclusions

In this chapter, procedure for a 2D heterogeneous model development in COMSOL was described with the help of the field validated 3D model outlined in Chapter 3. Permeability distributions were inputted into the 2D model to represent vertical soil profiles of two aquifers of varying permeability, Borden, and Swiss aquifers.

Simulations were run in the 2D heterogeneous model for both aquifers. While nZVI flux and other simulation parameters were identical for nZVI injection in both aquifers, the variance in permeability affected the results. The model result showed that nZVI distribution in the Swiss aquifer is more dispersed than in the Borden aquifer as the Swiss aquifer has higher variance in soil permeability. In addition, it is found that in Swiss aquifer, nZVI moves in the preferential flow paths (characterized by high permeability zones). Similar results are seen for different realizations of both aquifers and therefore it can be concluded that nZVI distribution is likely to be impacted by subsurface heterogeneity. This 2D heterogeneous model was used to perform a statistical analysis of nZVI transport parameters in the following chapter.

Chapter 5 Sensitivity Analysis

In this chapter, the analysis of variance (ANOVA) was performed to analyze the effect of various factors (injection rate, solution viscosity, aquifer velocity and lag period) on nZVI transport parameters (i.e., the center of mass and nZVI spread in both the x and z directions and nZVI attachment). The nZVI transport parameters were calculated by changing the value of one of the factors at a time and the effect of the change was evaluated by ANOVA.

5.1 One-Factor Analysis of Variance

The one-factor ANOVA is a statistical method that calculates the impact of one-factor. The one-factor ANOVA can be represented as follows (Montgomery and Runger 2007):

$$x_{ij} = \mu + \tau_i + \epsilon_{ij} \qquad (\mathbf{5-1})$$

Where x_{ij} is the value of random variable at j^{th} observation under i^{th} factor, μ is the overall mean, τ_i is the factor effect, and ϵ_{ij} is the random error component (Montgomery and Runger 2007). In this study, x_{ij} is the random variable which defines nZVI transport distance or spread, while the factors (τ_i) are groundwater velocity, and injection rate and viscosity. The analysis assumes that the observations are done in a random order and the effect of a factor is quantified by the null hypothesis.

5.1.1 Null Hypothesis

Let us consider parameter distributions where τ_1 and τ_2 are factors and the mean of these two distributions are μ_1 and μ_2 respectively. Now, the null hypothesis (H_0) can be written as follows (Montgomery and Runger 2007):

$$H_0: \mu_1 = \mu_2 \qquad (\mathbf{5-2})$$

This states that the means are statistically equal. To test this hypothesis, the statistical Fisher (F) test was performed, and the results are given in terms of the P value. To check the null hypothesis, a statistically significant/confidence level of 0.05 was used. In other words, if the P value > 0.05 then the null hypothesis cannot be rejected, and we do not have sufficient evidence to reject the null hypothesis and therefore the factor has no significant effect on the parameter. If the P value $\leq$ 0.05 then the null hypothesis is rejected meaning that means are statistically unequal, and factor has a significant effect on the parameter.

5.2 Estimation of Center of Mass and nZVI Spread

In order to assess the effect of the different factors on nZVI transport in aquifers of variable permeability, and to quantify the movement and shape of the mass distributions, various mass parameters were used including the center of mass and mass spread in a 2D domain. Both parameters were considered in two directions (i.e., x and z directions) and are shown in Figure 5.1.

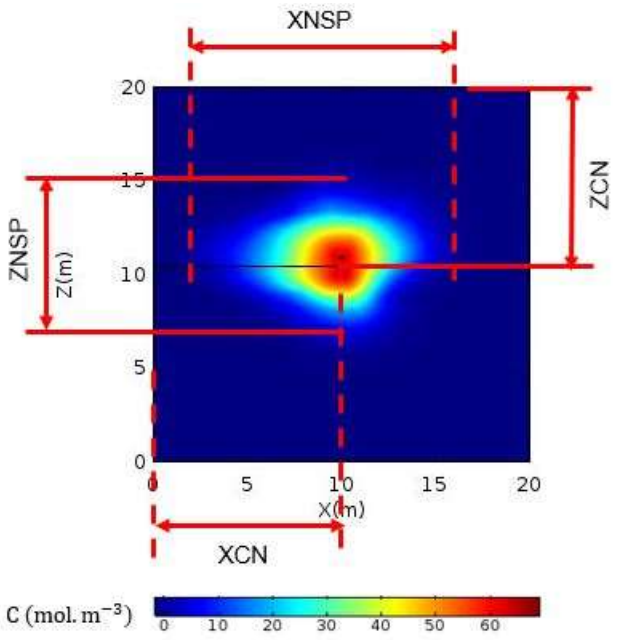

Figure 5.1: Measurement of center of nZVI mass and spread; XCN and ZCN are the center of mass in the x and z directions, respectively; XNSP and ZNSP are the spread of mass in the x and z directions, respectively.

These parameters (center of mass and mass spread) were based on the study of Dekker and Abriola (2000) and Krol (2011) and modified for this study. The horizontal center of mass (XCN) of the system was calculated as follows:

$$\mathrm{XCN} = \left(\frac{1}{\mathrm{M}}\right)\int \mathrm{x}.\,\mathrm{dm} \qquad (\mathbf{5-3})$$

Where, M is the total mass of nZVI, x is the distance in the x direction and dm is the incremental portion of the nZVI mass. The spreading of the mass (XNSP) was determined by the radius of gyration which can be determined as follows (Dekker and Abriola 2000):

$$\mathrm{XNSP} = \sqrt{\frac{\mathrm{I_Z^M}}{\mathrm{M}}} \qquad (\mathbf{5-4})$$

Where $\mathrm{I_Z^M}$ is the second moment of the mass about the z axis and is defined as:

$$\mathrm{I_Z^M} = \int (\mathrm{XCN} - \mathrm{x})^2 . \mathrm{dm} \qquad (\mathbf{5-5})$$

Where $(\mathrm{XCN} - \mathrm{x})$ is the distance of spread from the z axis passing through the center of nZVI mass. The vertical mass parameters (i.e., the center of nZVI mass in Z direction (ZCN) and mass spread in Z direction (ZNSP)) were calculated in a similar manner.

The total attachment $(\mathrm{S_T})$ $(\mathrm{mol.kg^{-1}})$ in the heterogeneous porous media due to nZVI injection was also evaluated. Recalling Eq. 2-17:

$$\frac{\rho_\mathrm{b}}{\theta}\frac{\partial \mathrm{S}}{\partial \mathrm{t}} = \mathrm{k_{att}C} \qquad (\mathbf{5-6})$$

Where, ρ_b is the density of porous media $(\mathrm{kg.m^{-3}})$, θ is the porosity $(-)$, S is the attached concentration $(\mathrm{mol.kg^{-1}})$, C is the aqueous nZVI concentration $(\mathrm{mol.m^{-3}})$, $\mathrm{k_{att}}$ is the attachment rate coefficient (s^{-1}). Implementing this equation into COMSOL, total attachment $(\mathrm{S_T})$ $(\mathrm{mol.kg^{-1}})$, can be calculated as follows:

$$\mathrm{S_T} = \int \partial \mathrm{S} = \theta \int (\frac{\mathrm{k_{att}C}}{\rho_\mathrm{b}})\mathrm{dt} \qquad (\mathbf{5-7})$$

5.3 Selection of Factors for Sensitivity Analysis

The one-factor ANOVA was performed on three factors: porewater velocity, injection flux, and viscosity of injected solution. These factors were chosen as they have been seen by others to have possible effects on nZVI transport. For example, Kocur et al. (2014) conducted a field scale test of nZVI injection in a contaminated sandy subsurface and found that field nZVI travel distance and longevity can be achieved with very high porewater velocities and highly stable nZVI suspensions. In addition, according to Henn and Waddill (2006), high porewater velocity and change in groundwater flow direction due to recirculation made it possible to distribute nZVI solution over the treatment area.

Injection mass flux is proportional to injection concentration and injection rate (Eq. (3-18)). Chowdhury et al. (2015) predicted through a CompSim simulation that injecting a higher volume of nZVI suspension (14 times greater) resulted in a 1.3 time increase in nZVI travel distance. Krol et al. (2013) also showed nZVI travel distance is affected by injection type (constant head or constant flux), and thereby injection rate. In addition, lag phase during successive injection of nZVI (i.e., the time when injection velocity is zero) can lead to deposition of nZVI in porous media under low porewater velocity conditions (Bennett et al. 2010, Kocur et al. 2014) and make nZVI immobile (Krol et al. 2013).

nZVI travel distance can also be influenced by the solution viscosity (Krol et al. 2013, Chowdhury et al. 2015). Krol et al (2013) showed that increasing solution

viscosity during constant flux injection affects nZVI travel distance by decreasing nZVI attachment in porous media and altering the hydraulics of the system (i.e., change in flow field due to injection of viscous fluid). These factors can be independently controlled and do not depend on permeability or soil collector diameter.

Table 5.1 presents six simulated cases. Each case had a different specified porewater velocity, injection viscosity, or injection flux. The range of values was based on previous field deployment of nZVI (He et al. 2010 , Bennett et al. 2010, Kocur et al. 2013, Kocur et al. 2014, Krol et al. 2013, Chowdhury et al. 2015).

Case 1 is the base case. In case 2 and 3, the value of porewater velocity was changed (shaded with light blue color, Table 5.1). Flux was changed for cases 4 and 5 (shaded with light orange color, Table 5.1) and viscosity was changed for case 6 (shaded with light green, Table 5.1) while the other factors were kept constant.

Table 5.1 Simulated cases for one-factor ANOVA

Case	Porewater velocity $(\mathbf{m.day^{-1}})$	Flux $(\mathbf{mol.m^{-2}s^{-1}})$	Viscosity $(\mathbf{Pa.s})$
1	0.1	0.009	0.013
2	1.5	0.009	0.013
3	10	0.009	0.013
4	0.1	0.022	0.013
5	0.1	0.900	0.013
6	0.1	0.009	0.072

The values of porewater velocities were chosen for cases 1 and 2 based on data found from field injection studies. These porewater velocities were estimated during field injection of nZVI in a shallow granulated aquifer by Bennett et al. (2010) and used in a modeling study by Krol et al. (2013). Case 3 uses a porewater velocity of 10 $(\mathrm{m.day^{-1}})$ which is 100 times greater than the porewater velocity used in case 1. This value was used to provide an upper bound to the simulations and corresponds to a very fast-moving gravel/sand aquifer (approximate groundwater (Darcy) velocity of 3.6 $(\mathrm{m.day^{-1}})$).

The nZVI injection flux values were also chosen from the field injection data. Case 1 has a flux value of 0.009 $(\mathrm{mol.m^{-2}s^{-1}})$ corresponding to an injection of 0.96 $(\mathrm{g.L^{-1}})$ nZVI (Krol et al. 2013, Chowdhury et al. 2015) and case 4 accounts for an increased flux value of 0.022 $(\mathrm{mol.m^{-2}s^{-1}})$ for an injection of 2.5 $(\mathrm{g.L^{-1}})$ nZVI (Kocur et al. 2013). Case 5 uses a flux value of 0.900 $(\mathrm{mol.m^{-2}s^{-1}})$ which is 100 times greater than the flux used in case 1. This represents an upper bound of the flux, chosen to observe the sensitivity of injection flux on nZVI transport.

CMC-nZVI solutions are typically injected at two viscosity values: 0.013 and 0.072 $(\mathrm{Pa.s})$, corresponding to the molecular weight of the polymer, 90,000 $(\mathrm{g.mol^{-1}})$ (CMC 90K) and 250,000 $(\mathrm{g.mol^{-1}})$ (CMC 250K), respectively. Both of these viscosity values were used by Krol et al. (2013) in their modeling study, while CMC 90K was used by He et al. (2009) and Raychoudhury et al. (2012) in their experimental investigations. CMC 250K was used to stabilize nZVI suspension by

others (He and Zhao 2007, Sakuchaicharoen et al. 2010). These two CMC values were used in this study.

5.4 One-Factor ANOVA Results

The one-factor ANOVA was performed on both aquifers by changing the values of porewater velocity, flux, and viscosity as outlined in Table 5.1. To examine the effect of porewater velocity, cases 1, 2 and 3 were simulated for 15 permeability realizations. Similarly, to find out the effect of flux, cases 1, 4, and 5 were used, while cases 1 and 6 were used to examine the effect of viscosity.

The resulting P-values are presented in Table 5.2 while Figures 5.2, 5.3 and 5.4 show the box plots for each of the calculated parameters for both aquifers. The median of the box plot is represented by a central mark, while the upper and lower edges of the box plot represent the upper and lower quartiles, respectively. The tails of the distribution are represented by whiskers of the box plot.

Table 5.2 P Values and trends for one-factor ANOVA (at 48 hours)

	Porewater velocity				**Flux**				**Viscosity**			
	Borden		**Swiss**		**Borden**		**Swiss**		**Borden**		**Swiss**	
	P	**T**	**P**	**T**	**P**	**T**	**P**	**T**	**P**	**T**	**P**	**T**
XCN	**0.002**	+0.2	0.094		0.991		0.978		0.796		0.849	
XNSP	0.959		0.978		0.404		0.960		**8E-09**	+0.8	**0.012**	+0.5
ZCN	0.998		0.988		0.997		0.999		0.986		0.933	
ZNSP	0.898		0.805		0.219		0.584		**6E-10**	+0.7	**1E-05**	+0.7
S_T	0.303		0.199		**8E-116**	+0.6	**5E-83**	+0.6	**2E-15**	**-4E-4**	**2E-09**	**-5E-4**

Note: P = P values, T = trend of the median values where $(+/-)$ indicate an increasing or decreasing trend with increasing porewater velocity, flux or viscosity values; Shaded values indicate P values equal to or below 0.05; P values close to 0.05 are indicated by light green shade.

5.4.1 Effect of Porewater Velocity

To find whether the effect of the porewater velocity is statistically significant, case 1, 2, and 3 were simulated for 15 random permeability distributions of both aquifers. While case 1 uses a porewater velocity of 0.1 $(\mathrm{m.day^{-1}})$, case 2 uses 1.5 $(\mathrm{m.day^{-1}})$ (Krol et al. 2013) and case 3 uses a porewater velocity of 10 $(\mathrm{m.day^{-1}})$ which is 100 times greater than the porewater velocity used in case 1. Figure 5.2 shows the effect of the porewater velocity on XCN, XNSP, ZCN, ZNSP and $\mathrm{S_T}$.

As seen in Figure 5.2, there is very little or no change in median irrespective of the aquifer for shifting porewater velocity from 0.1 $(\mathrm{m.day^{-1}})$ to 1.5 $(\mathrm{m.day^{-1}})$. However, changes were observed when the porewater velocity was increased by 100 to a porewater velocity of 10 $(\mathrm{m.day^{-1}})$, particularly in case of XCN, XNSP and $\mathrm{S_T}$. However, P value was less than the significant level of 0.05 for the centre of mass of the Borden aquifer only (Table 5.2). Therefore, the null hypothesis can be rejected for this case only. For all other distributions, the P value ranges between (0.094 to 0.998), which is greater than the significant level of 0.05 and therefore the null hypothesis cannot be rejected.

In other words, the change in mentioned values of porewater velocity does not have a statistically significant effect on nZVI transport (in terms of movement, spread, and nZVI attachment onto porous media) except for nZVI mass movement in X direction for the Borden aquifer.

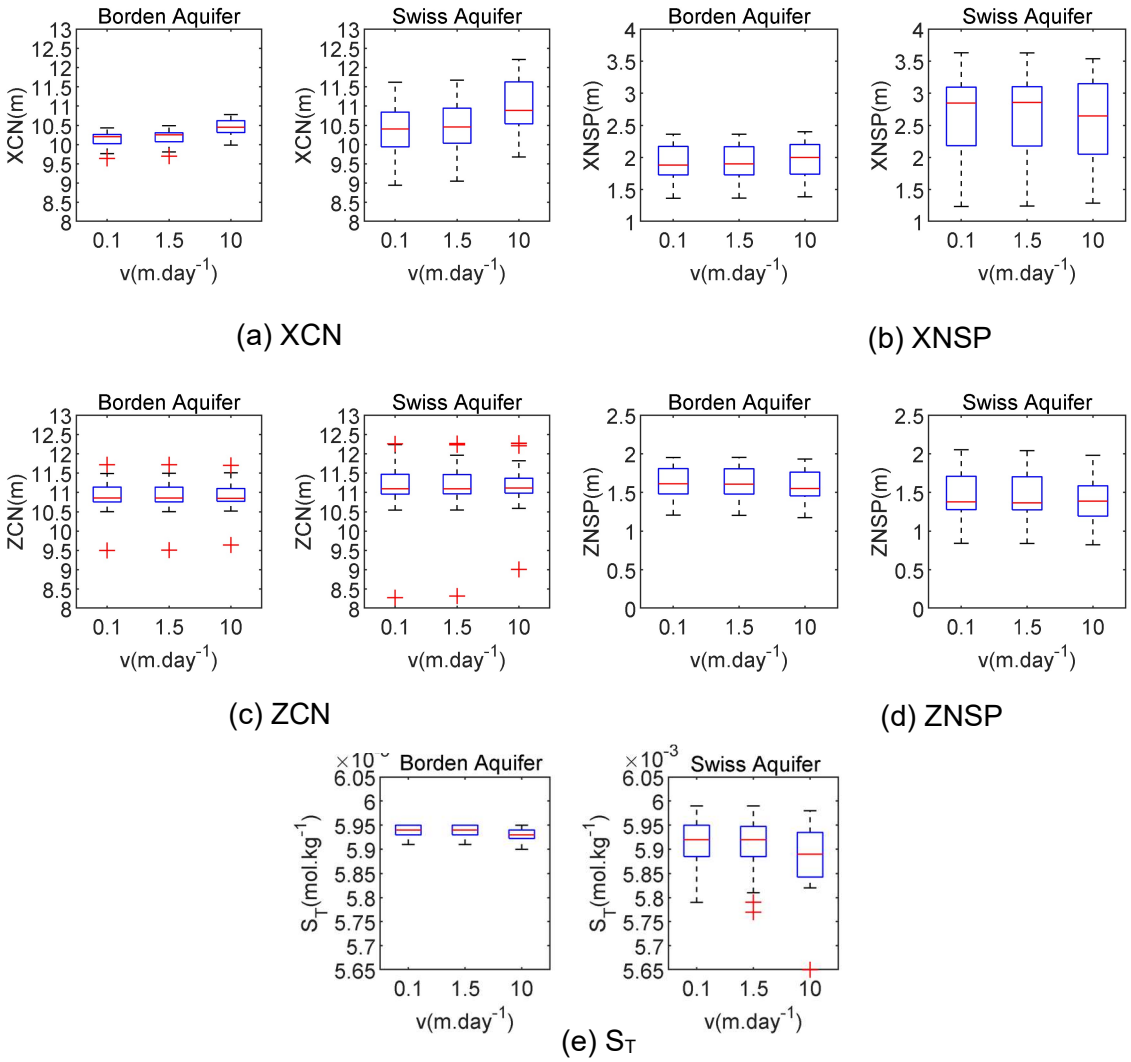

Figure 5.2: Effect of porewater velocity on: (a) center of nZVI mass in X direction (XCN) (b) mass spread in X direction (XNSP) (c) center of nZVI mass in Z direction (ZCN) (d) mass spread in Z direction (ZNSP) (e) nZVI attachment (S_T); at 48 hours

It is likely that no significant impact is seen in the Swiss aquifer due to the larger dispersion caused by increased heterogeneity which would overshadow the result of the higher porewater velocity. This is confirmed by the relatively low P-value for the Swiss XCN (P value is 0.094, very close to significance level 0.05)

showing that heterogeneity may have had an impact on the distribution. To check whether heterogeneity impacts pore water velocity a two factor ANOVA is necessary which considers the interaction effect between these factors.

These results differ from others reported for several reasons. In some laboratory column studies (Kanel et al. 2007, He et al. 2009, Phenrat et al. 2009), porewater velocity ranged from 15 $(\mathrm{m.day^{-1}})$ to 100 $(\mathrm{m.day^{-1}})$ which is higher than the upper bound used in this study. For example, He et al. (2009) reported 0.16 m CMC-nZVI travel distance using 0.1 $(\mathrm{m.day^{-1}})$ porewater velocity and 146 m travel distance for porewater velocity of 61 $(\mathrm{m.day^{-1}})$ in their experimental and modeling study. Similarly, Johnson et al. (2009) used three porewater velocities (i.e., 8.6,25.9 and 86.4 $(\mathrm{m.day^{-1}})$) during column experiment which don't represent field porewater velocity and are higher than the velocities used in this study. Tiraferri and Sethi (2008) used a water-saturated sand-packed column for transport experiments of guar gum coated nZVI and noted that transport increased when porewater velocity increased from 2.38 $(\mathrm{m.day^{-1}})$ to 11.9 $(\mathrm{m.day^{-1}})$. However, these results are qualitative and do not represent a statistically significant effect. Lastly, Kocur et al. (2014) reported a 1 m travel distance of CMC-nZVI under a porewater velocity of 0.1 $(\mathrm{m.day^{-1}})$ which supports the result of this study (Figure 5.2).

5.4.2 Effect of Injection Flux

To find whether the effect of the nZVI injection flux has a statistically significant effect on nZVI transport, cases 1, 4, and 5 were simulated for 15 random permeability distributions of both aquifers. While case 1 uses an injection flux of 0.009 $(\mathrm{mol.m^{-2}s^{-1}})$ corresponding to a nZVI injection of 0.96 $(\mathrm{g.L^{-1}})$ at a rate of $5.67 \times 10^{-5}(\mathrm{m^3.s^{-1}})$ (Krol et al. 2013, Chowdhury et al. 2015), case 4 uses an increased flux value of 0.022 $(\mathrm{mol.m^{-2}s^{-1}})$ for nZVI injection of 2.5 $(\mathrm{g.L^{-1}})$ (Kocur et al. 2013) and case 5 uses a flux value of 0.900 $(\mathrm{mol.m^{-2}s^{-1}})$ which is 100 times greater than the flux used in case 1. Figure 5.3 shows the effect of these injection flux values on XCN, XNSP, ZCN, ZNSP and $\mathrm{S_T}$.

As seen in Figure 5.3, all the box plots have very little or no change in median irrespective of the aquifer when the injection flux is raised from 0.009 $(\mathrm{mol.m^{-2}s^{-1}})$ to 0.022 $(\mathrm{mol.m^{-2}s^{-1}})$. However, some change is observed when the injection flux is increased to 0.9 $(\mathrm{mol.m^{-2}s^{-1}})$, particularly for the XNSP in Borden, and ZNSP and $\mathrm{S_T}$ for both aquifers. However, the ANOVA analysis shows that the P value is less than the significant level of 0.05 only in case of nZVI attachment for both aquifers (Table 5.2). Therefore, the null hypothesis can be rejected only for this case. In other words, the change in nZVI injection flux does not have a statistically significant effect on nZVI transport (in terms of movement and spread of nZVI in porous media) but does have a statistically significant effect on nZVI attachment.

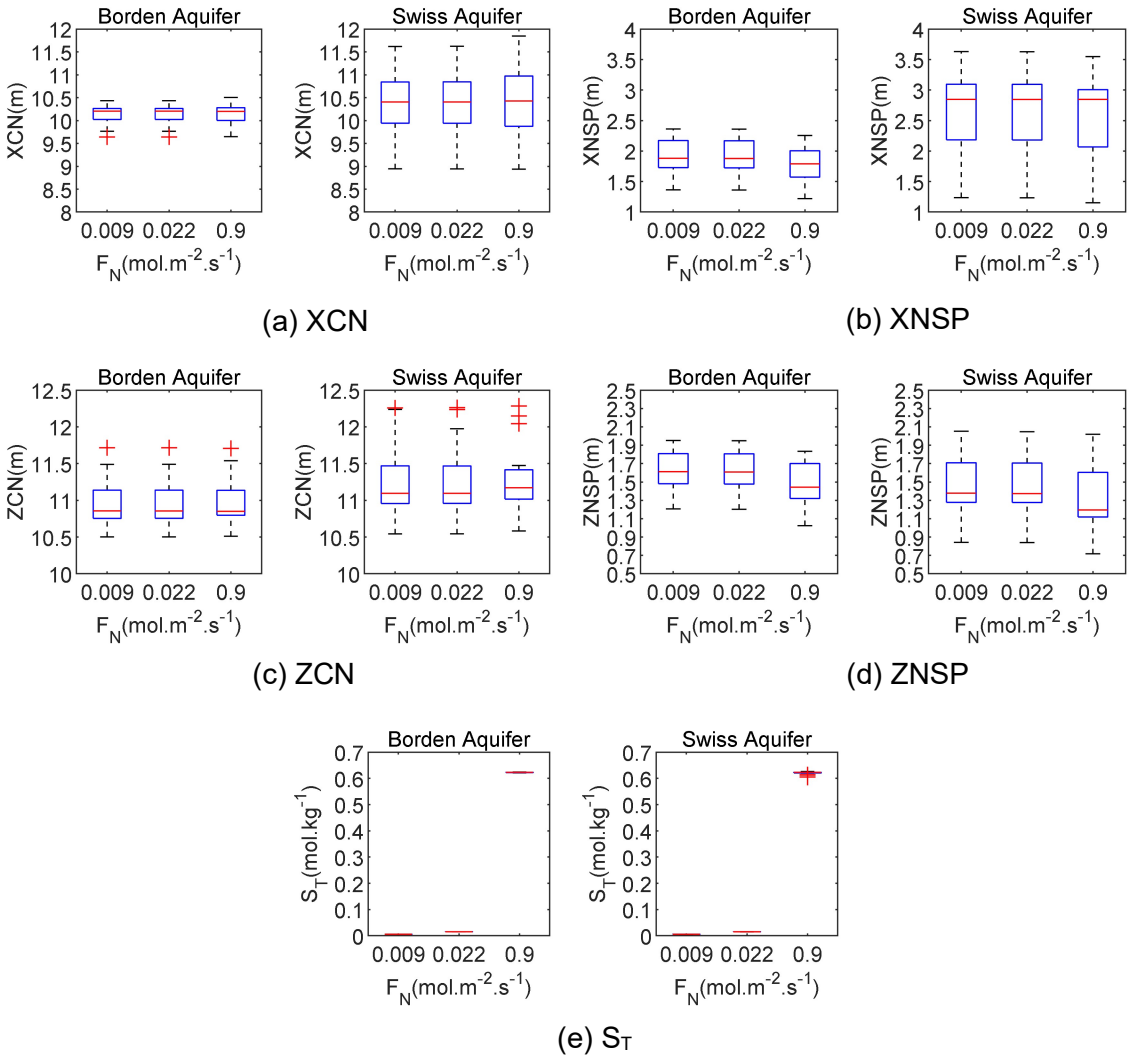

Figure 5.3: Effect of nZVI injection flux on: (a) center of nZVI mass in X direction (XCN) (b) mass spread in X direction (XNSP) (c) center of nZVI mass in Z direction (ZCN) (d) mass spread in Z direction (ZNSP) (e) nZVI attachment (S_T); at 48 hours

However, this statistically significant effect is likely due to the larger hypothetical flux 0.9 $(\mathrm{mol.m^{-2}s^{-1}})$ while small differences were observed due to an increase in field flux from 0.009 $(\mathrm{mol.m^{-2}s^{-1}})$ to 0.022 $(\mathrm{mol.m^{-2}s^{-1}})$ (Figure 5.3 (e)). It is interesting to note that the increased injection flux, increases the total

attached mass (S_T). This is contrary to what is typically shown. As injection flux is increased, the porewater velocity near the well increases, which would lead to decreased attachment rate (Krol et al, 2013). However, as flux is increased, the amount of mass injected into the system increases, therefore, there is more mass that can be attached.

5.4.3 Effect of Subsurface Viscosity

To find whether the effect of the subsurface viscosity is statistically significant, cases 1 and 6 were simulated for 15 random permeability distributions of both aquifers. While case 1 uses a solution viscosity of 0.013 $(\mathrm{Pa.s})$, case 6 uses a solution viscosity 0.072 $(\mathrm{Pa.s})$ (He and Zhao 2007, He et al. 2009, Sakulchaicharoen et al. 2010, Raychoudhury et al. 2012, Krol et al. 2013). Figure 5.4 shows the effect of increasing the viscosity on the XCN, XNSP, ZCN, ZNSP and S_T.

As seen in Figure 5.4, a change in viscosity leads to a change in the median in almost all the parameters, with the largest difference being observed for nZVI mass spread in both directions $(\mathrm{XNSP\ and\ ZNSP})$ and nZVI attachment (S_T). The P values concur with this visual inspection, with P<0.05 being calculated for nZVI mass spread in both directions $(\mathrm{XNSP\ and\ ZNSP})$ and nZVI attachment for both aquifers (Table 5.2). For all other distributions, the P values ranges from (0.796 to 0.986) which is greater than the significant level of 0.05 and therefore the null hypothesis cannot be rejected. In other words, the change in mentioned field scale

values of viscosity have a statistically significant effect on nZVI transport in terms of spread of nZVI in porous media and nZVI attachment but have no statistically significant effect on nZVI center of mass.

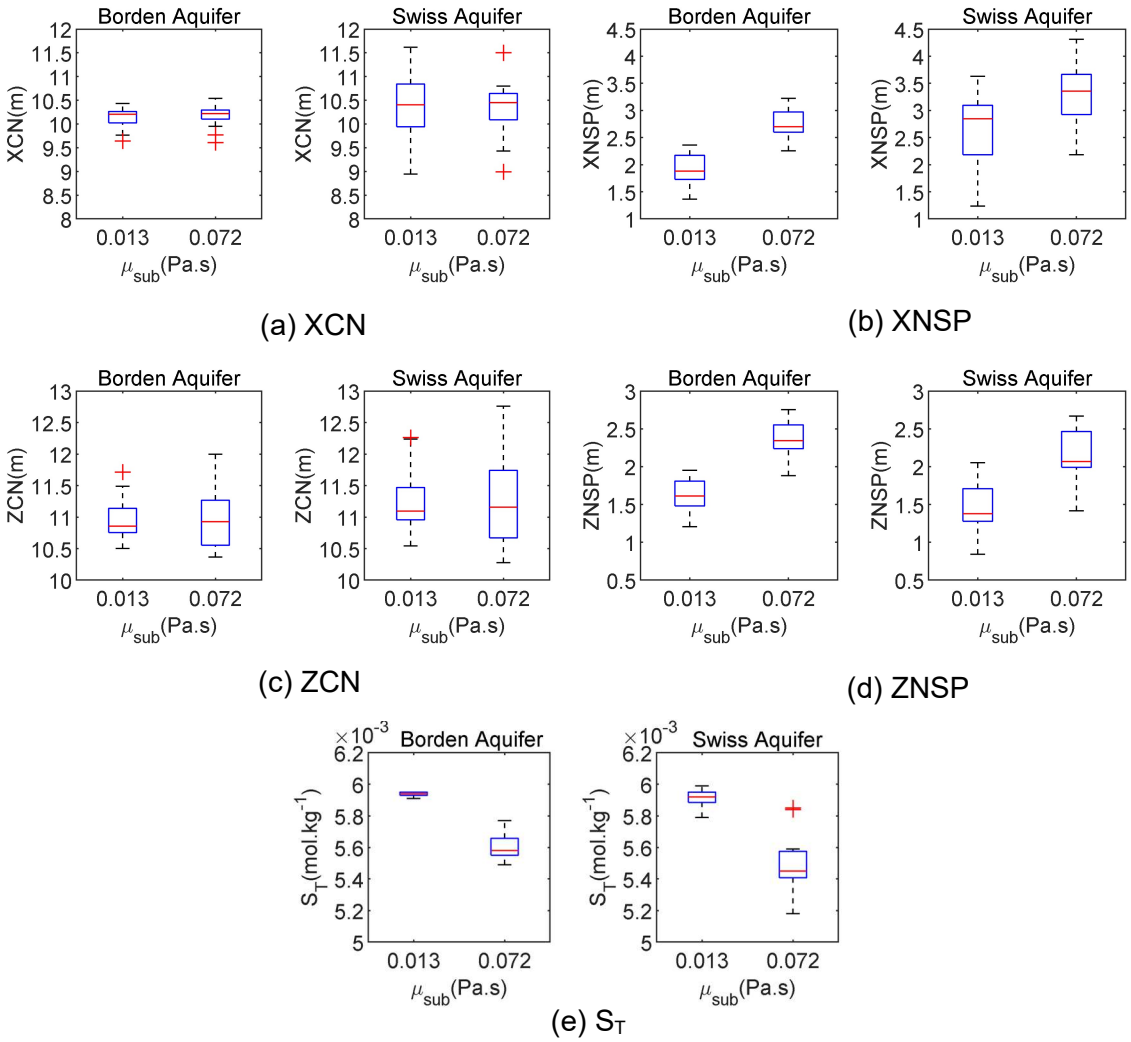

Figure 5.4: Effect of subsurface viscosity on: (a) center of nZVI mass in X direction (XCN) (b) mass spread in X direction (XNSP) (c) center of nZVI mass in Z direction (ZCN) (d) mass spread in Z direction (ZNSP) (e) nZVI attachment

Figures 5.5 (a) and (b) show two simulations for Borden aquifer at 48 hours for case 1 (viscosity 0.013 $(\mathrm{Pa.s})$) and case 6 (viscosity 0.072 $(\mathrm{Pa.s})$) respectively. It is clear from Figure 5.5 (b) that although the centre of mass is comparable, nZVI spread has been increased due to change in viscosity from 0.013 $(\mathrm{Pa.s})$ to 0.072 $(\mathrm{Pa.s})$ which is supported by the change in attached mass distribution (i.e., Figure 5.6). As the spread of nZVI mass increases, attachment decreases (Figure 5.6).

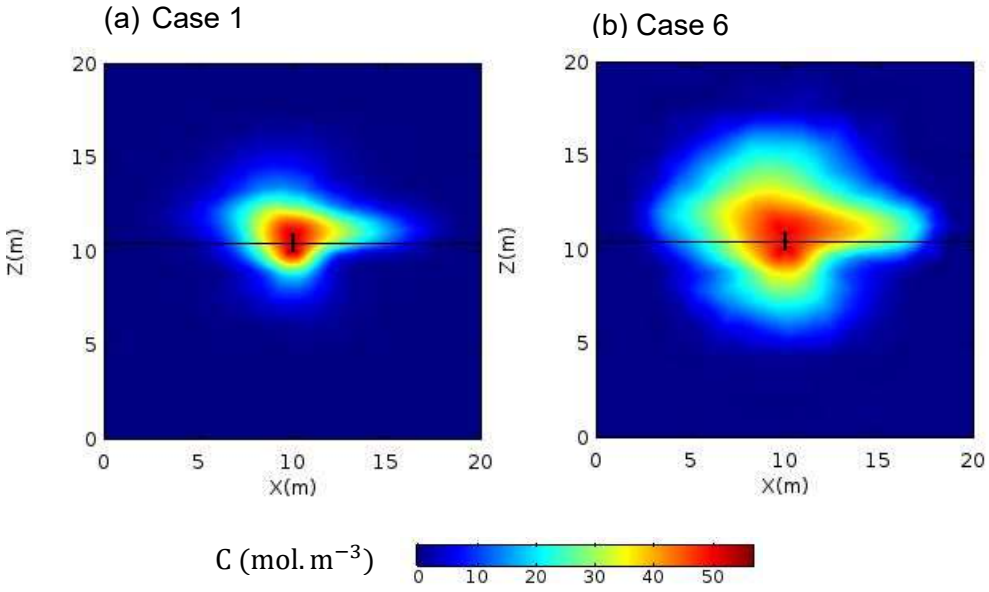

Figure 5.5: nZVI distribution in the Borden aquifer for (a) Case 1, viscosity 0.013 $(\mathbf{Pa.s})$ (b) Case 6, viscosity to 0.072 $(\mathbf{Pa.s})$; at 48 hours

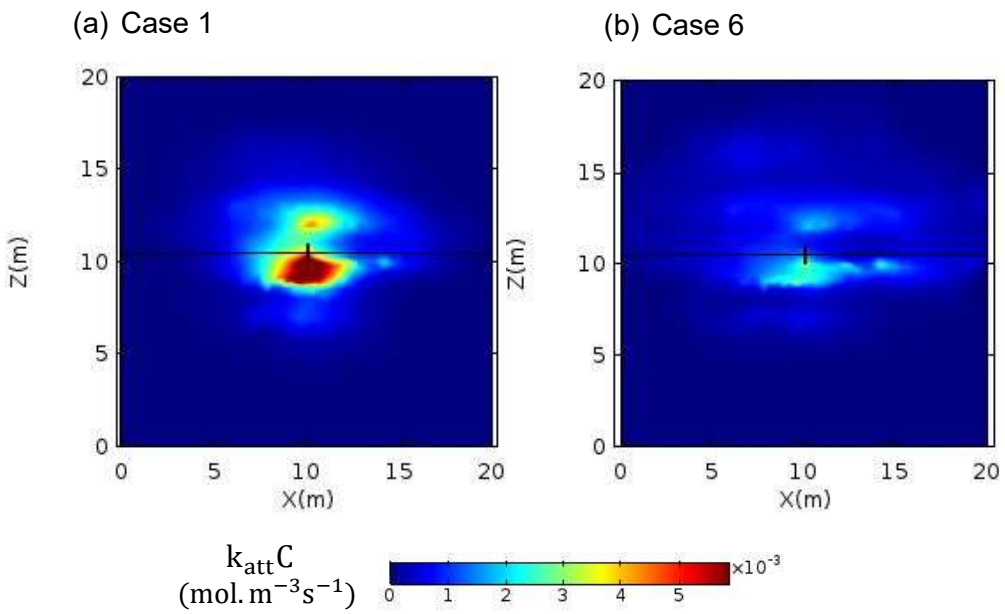

Figure 5.6: nZVI attached concentration in the Borden aquifer for (a) Case 1 viscosity 0.013 ($\mathbf{Pa.s}$) (b) Case 6, viscosity to 0.072 ($\mathbf{Pa.s}$); at 48 hours

It can be concluded that, among the three factors considered for one-factor ANOVA analysis, injection viscosity has a statistically significant effect on nZVI spread and attachment in the subsurface porous media, while field scale porewater velocity and injection flux do not change the nZVI distribution parameters significantly (i.e., movement and spread) and have no statistically significant effect on nZVI spread even with a large magnitude. The one exception is the horizontal center of mass in the Borden aquifer that was affected by a hypothetical large porewater velocity which likely due to the low degrees of heterogeneity in Borden as compared to the Swiss aquifer.

5.4.4 Effect of Lag Period

A lag period is the interval between two successive nZVI injections. During this period, nZVI flux is zero and injected nZVI mass from the previous injection may be affected by reduced groundwater velocity caused by the stoppage. Lag phase during successive injection of nZVI can lead to nZVI deposition onto the porous media under low porewater velocity (Bennett et al. 2010, Kocur et al. 2014) and make nZVI immobile (Krol et al. 2013).

To find out the effect of lag period on nZVI mass movement, spread and attachment, the one-factor ANOVA was performed for three different cases where case A (base case) considers 48 hours of constant flux nZVI injection, followed by a 48 hours of zero flux (or lag phase) for a total of 96 hours; case B considers intermittent nZVI injection of 24 hours and lag phase of 24 hours for a total of 96 hours; case C considers successive constant flux nZVI injection of 12 hours and lag phase of 12 hours for a total of 96 hours (Table 5.3). Case A has the longest continual injection phase (48 hours) and lag phase (48 hours) compared to case B and C, however in total all cases have the same hours of injection and lag period (48 hours of each). This results in the same amount of total nZVI injected. The porewater velocity before and during lag period for all the cases was kept the same ($0.1\ (\mathrm{m.day^{-1}})$) and the viscosity of injected solution was maintained at 0.013 Pa.s.

Table 5.3 : Simulated case for ANOVA considering lag period

Case	Time $(\mathbf{h})$	Porewater velocity $(\mathbf{m.day^{-1}})$	Flux $(\mathbf{mol.m^{-2}s^{-1}})$	Viscosity $(\mathbf{Pa.s})$
A	0-48	0.1	0.009	0.013
	48-96	0.1	**0.0**	0.013
B	0-24	0.1	0.009	0.013
	24-48	0.1	**0.0**	0.013
	48-72	0.1	0.009	0.013
	72-96	0.1	**0.0**	0.013
C	0-12	0.1	0.009	0.013
	12-24	0.1	**0.0**	0.013
	24-36	0.1	0.009	0.013
	36-48	0.1	**0.0**	0.013
	48-60	0.1	0.009	0.013
	60-72	0.1	**0.0**	0.013
	72-84	0.1	0.009	0.013
	84-96	0.1	**0.0**	0.013

The P values for this analysis were obtained for all variations of the three cases (A, B and C) and are shown in Table 5.4.

Table 5.4: P values and trends for one-factor ANOVA for lag period scenarios (at 96 hrs)

	C-A:C-B:C-C				C-A: C-B			
	Borden		Swiss		Borden		Swiss	
	P	T	P	T	P	T	P	T
XCN	0.674		0.831		0.609		0.733	
XNSP	0.317		0.789		0.567		0.824	
ZCN	0.955		0.992		0.869		0.953	
ZNSP	0.920		0.874		0.744		0.658	
S_T	**6E-22**	+8E-4	**1E-11**	+7E-4	**4E-12**	+4E-4	**3E-6**	+4E-4

	C-A:C-C				C-B: C-C			
	Borden		Swiss		Borden		Swiss	
	P	T	P	T	P	T	P	T
XCN	0.397		0.554		0.719		0.798	
XNSP	0.139		0.503		0.348		0.655	
ZCN	0.766		0.901		0.891		0.946	
ZNSP	0.997		0.668		0.699		0.975	
S_T	**1E-18**	+8E-4	**6E-11**	+7E-4	**6E-9**	+4E-4	**4E-4**	+3E-4

Note: P = P values, T = trend of the median values where $(+/-)$ indicate an increasing or decreasing trend due to lag effect of zero flux; Shaded values indicate P values equal to or below 0.05.

Figure 5.7 shows the effect of lag period on XCN, XNSP, ZCN, ZNSP and S_T. As seen in Figure 5.7, switching to lag period leads to a change in the median in almost all the parameters, with the largest difference being observed for nZVI attachment (S_T). P values are measured for a combination of cases (Table 5.4). For all combinations, one-factor ANOVA results in $P \leq 0.05$ for attachment only and null hypothesis can be rejected. For all other distributions, the P value ranges between (0.139 to 0.997) which is greater than the significant level of 0.05 and therefore the null hypothesis cannot be rejected.

In other words, the lag period has a statistically significant effect on nZVI attachment. Less attachment has been observed in case of longer continual injection and lag periods (i.e., case A) compared to other cases (i.e., Case B and C). Longer injection periods (case A) increased the horizontal spread of the nZVI plume (XNSP) in both aquifers (Figure 5.7 (b)) and larger spread means smaller attachment (Figure 5.7(e)). In addition, more lag phases in cases B and C impacted the continuity of the injection period and hence nZVI travel distance. Case B has 2 lag phases and case C has four lag phases. Each lag phase increases nZVI attachment, resulting in the highest attachment rate for the case C scenario. Although the number of injection periods increases in case B and case C compared to case A, the duration of injection becomes shorter and the total amount of time for injection is the same for all three cases. Nonetheless, these results show that the total time of injection is not as important as the number of lag

periods and successive injection and lag periods of shorter duration led to greater nZVI attachment.

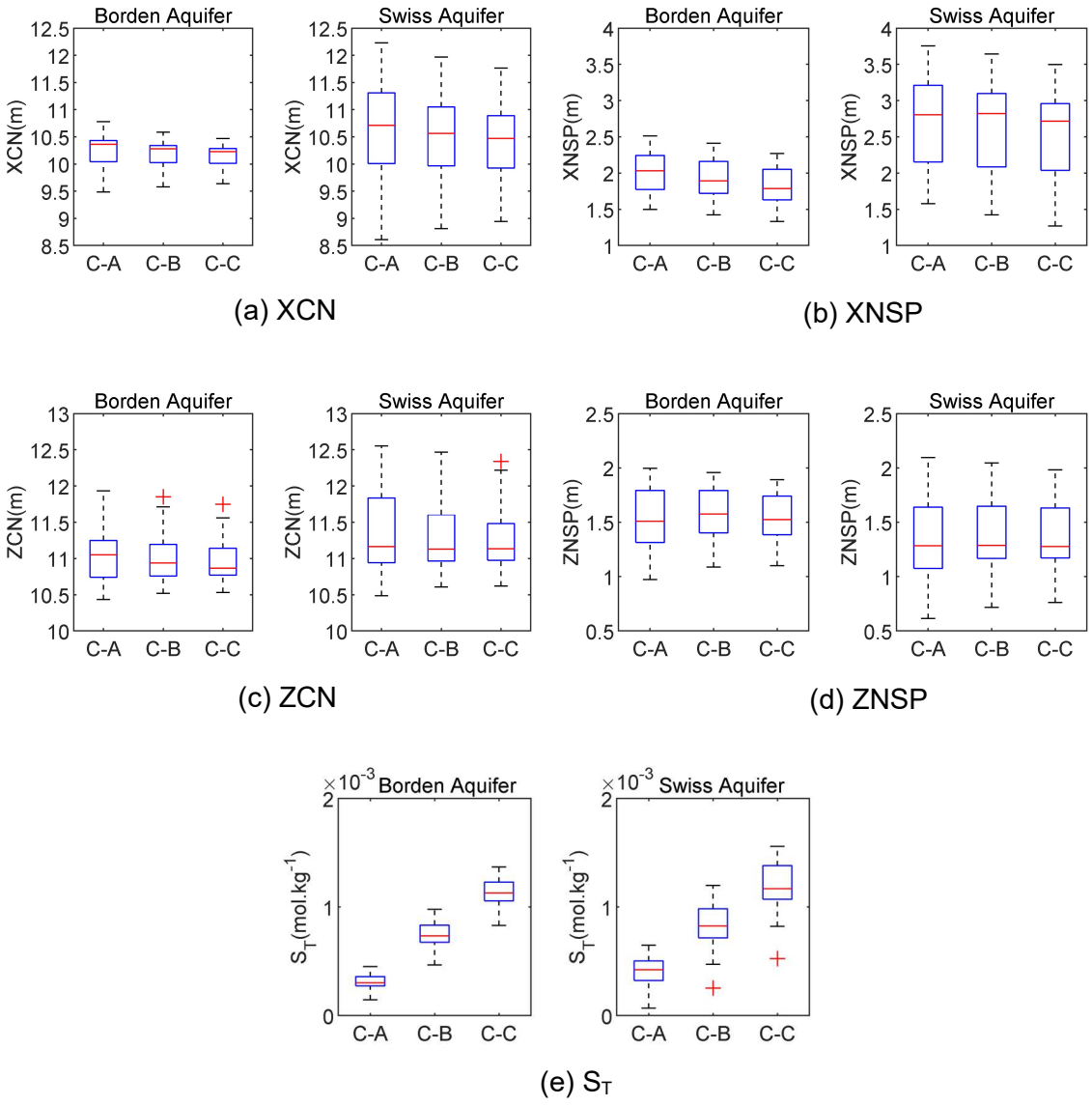

Figure 5.7: Effect of lag period on: (a) center of nZVI mass in X direction (XCN) (b) mass spread in X direction (XNSP) (c) center of nZVI mass in Z direction (ZCN) (d) mass spread in Z direction (ZNSP) (e) nZVI attachment (S_T); at 96 hours (C-A: Case A, C-B: Case B, C-C: Case C)

As less nZVI attachment is desired for optimum transport in porous media, long injection periods followed by short lag phase is recommended for nZVI deployment.

5.4.5 Effect of Heterogeneous Permeability Distribution

All simulations were run in two heterogeneous aquifers: Borden and Swiss. Although the mean permeability, correlation length, and porosity are same for both aquifers, the Swiss aquifer has a higher variance in permeability resulting in a greater contrast in permeability fields. In this way, the Swiss aquifer is more heterogeneous than the Borden aquifer. Overall, heterogeneity of both aquifers impacted the distribution of parameters as seen from the box plot distributions (i.e., Figure 5.2, Figure 5.3, Figure 5.4, Figure 5.7). For all cases, it was observed that the variance of the parameters (i.e., the center of mass, spread, and nZVI attachment) are higher in Swiss aquifer than in the Borden aquifer (i.e., the variance of XCN distribution in Borden aquifer due to 0.1 $(\mathrm{m.day^{-1}})$ porewater velocity is 0.05 but in Swiss aquifer, it is 0.53).

5.5 Conclusions

In this chapter, the one-factor ANOVA analysis was performed on various parameters while changing three factors: porewater velocity, injection flux, and injection viscosity. Procedure for estimating center of mass, spread of mass and nZVI attachment was explained and selection of factors was outlined.

The factors chosen were porewater velocity, injection flux, and injection viscosity and their effects on mass transport were analyzed and plotted using box plot distributions. The one-factor ANOVA analysis showed that the field porewater velocity did not have a statistically significant effect on nZVI movement and spread even with increased magnitude (a porewater velocity 100 times larger than typical field scale value), except on the horizontal center of mass in the Borden aquifer. This result shows that the porewater velocity induced by intrinsic groundwater velocity of the injection site is not an important factor for optimizing nZVI injection.

The injected nZVI flux also did not change the nZVI distribution parameters (i.e., movement and spread) even with a large magnitude (a flux of 100 times larger than a typical nZVI flux field scale value) but did have a statistically significant effect on nZVI attachment in both aquifers. However, this statistically significant effect is likely due to the largest flux (0.9 $(\mathrm{mol.\,m^{-2}s^{-1}})$) while a small difference was observed due to an increase of field flux. This result shows that injection flux is not an important factor for optimizing nZVI deployment in terms of travel distance but could be important for the amount of nZVI that gets attached, especially near the well head.

Injection solution viscosity had a statistically significant effect on nZVI mass spread and attachment in both aquifers, but no statistically significant effect was shown on the nZVI center of mass movement. This shows that viscosity is an important factor for optimizing nZVI deployment at the field scale. Stable nZVI

suspension using highly viscous polymer could increase nZVI spread and decrease attachment leading to a possible reduction in remediation time and overall cost.

The length of the injection and lag period change nZVI attachment by a large difference with fixed field scale porewater velocity (i.e., 0.1 $(\mathrm{m.day^{-1}})$). The result indicates that the length of the injection and lag period are important factors for optimizing nZVI deployment at the field scale. Three types of lag periods (i.e., one 48 hours, two 24 hours and four 12 hours in a timeframe of 48 hours) have been simulated in the current work. Less attachment has been observed in case of longer continual injection and lag periods (48 hours) compared to shorter periods (24 hours and 12 hours). As less nZVI attachment is desired for optimum transport in porous media, long injection periods followed by short lag phase is recommended for nZVI deployment.

Heterogeneity of both aquifers impacted the nZVI distribution parameters as seen from the box plot distribution. For all cases, it has been observed that parameter variance (i.e., the center of mass, spread and attachment of nZVI) is higher in the Swiss aquifer than in the Borden aquifer as higher variance of permeability in Swiss aquifer has enabled these parameters to vary more.

This work aimed to answer some key questions regarding nZVI deployment in the field. During field-scale injection, maintaining nZVI injection flux, viscosity of nZVI solution, lag period, managing low to high porewater velocity condition

become key challenges for the engineers and decision makers. This work was aimed at finding the important factors for nZVI deployment to aid in field scale injection. While a large body of work by others has focused on finding the optimum injection flux or understanding how porewater velocity will affect treatment, this study shows that neither of these factors has a large impact on nZVI travel distance or spread. Therefore, maintaining a hydraulic gradient and associated porewater velocity during field injection is not important as porewater velocity does not change nZVI travel distance by a notable difference. These results are somewhat contrary to other studies which may be a result of varying input parameters (i.e. some studies used unrealistically high groundwater velocities) or due to the nature of the analysis. Although some studies reported an “effect” of various parameters on nZVI travel distance, the effects were never quantified and therefore are more qualitative. The study presented here quantifies the results using a statistical analysis. The important factors found are the injection viscosity, injection period and aquifer heterogeneity for optimizing nZVI deployment.

Chapter 6 Conclusions and Future Work

6.1 Conclusions

This thesis examined the impact of factors that may affect nZVI transport parameters in heterogeneous groundwater aquifers by performing a statistical analysis, the one factor ANOVA. This was done with the use of a developed 2D COMSOL model and the following conclusions were reached:

1. Field porewater velocity did not have a statistically significant effect on nZVI movement and spread, except on the horizontal center of mass in the Borden aquifer. This result shows that the porewater velocity is not an important factor for optimizing nZVI injection.
2. nZVI injection flux is not an important factor for optimizing nZVI deployment as nZVI flux did not change the nZVI distribution parameters (i.e., movement and spread) even with a large flux magnitude. However, large injection flux can cause accumulation of nZVI particles near the well head.
3. Injection solution viscosity had a statistically significant effect on nZVI mass spread and attachment in both aquifers but not on the nZVI center of mass. Higher subsurface viscosity was found to maximize nZVI spread and minimize nZVI attachment. This shows that viscosity is an important factor for optimizing nZVI deployment at the field scale. Stable nZVI suspension in the presence of highly viscous polymer should be used during field scale

injection to ensure optimum nZVI spread which could result in reducing remediation time.

4. The length of injection and lag period are important factors for optimizing nZVI deployment at the field scale. In this work, three types of lag periods were considered in a 48 hours timeframe. Less nZVI attachment occurred during long injection phase followed by a long lag periods (48 hours) compared to shorter lag periods (24 hours and 12 hours). It is recommended that long injection and short lag phase be used during nZVI deployment at the field scale which will result in less nZVI in the porous media.
5. Aquifer heterogeneity impacted the nZVI distribution parameters as seen from the box plot distribution. The variance of parameters (i.e., the center of mass, spread and attachment of nZVI) was higher in the Swiss aquifer than in the Borden aquifer for all cases. These parameters for Swiss aquifer varied more due to higher variance of permeability. To quantify the effect of soil heterogeneity on nZVI transport, a two-factor ANOVA analysis needs to be performed (outside the scope of this work).

6.2 Recommendations for Future Work

Future studies and research can be done in the following areas:

1) Two factor analysis of variance can be performed to understand the effect of soil permeability on nZVI transport.

2) A 3D model with 3D heterogeneous permeability field can be developed.
3) The current model considers nZVI transport through the subsurface without any reactivity. A reactive transport model would further add to nZVI optimization.
4) The current model considers nZVI transport for contaminant remediation in a saturated subsurface. Future studies could be performed in the unsaturated zone.

References

Alonso, U., Missana, T., Patelli, A., and Rigato, V. 2007. Bentonite colloid diffusion through the host rock of a deep geological repository. Physics and Chemistry of the Earth, Parts A/B/C, **32**(1): 469–476. doi:10.1016/j.pce.2006.04.021.

Asad, M.A., Krol, M., and Briggs, S. 2018. Nano zero valent iron (nZVI) remediation: A COMSOL modelling approach. Canadian Geotechnical Society (CGS) Conference(GeoEdmonton 2018).

Bennett, P., he, F., Zhao, D., Aiken, B., and Feldman, L. 2010. In situ testing of metallic iron nanoparticle mobility and reactivity in a shallow granular aquifer. Journal of contaminant hydrology, **116**: 35–46. doi:10.1016/j.jconhyd.2010.05.006.

Bhushan, B. 2000. Surface Roughness Analysis and Measurement Techniques. *In* Modern Tribology Handbook, Two Volume Set. CRC Press. doi:10.1201/9780849377877.ch2.

Brown, C.L., Pope, G.A., Abriola, L.M., and Sepehrnoori, K. 1994. Simulation of surfactant-enhanced aquifer remediation. Water Resources Research, **30**(11): 2959–2977. doi:10.1029/94WR01458.

Budtov, V.P. 1967. Study of the concentration dependence of the viscosity of dilute polymer solutions. Compression of polymer chains. Polymer Science U.S.S.R., **9**(4): 854–862. doi:10.1016/0032-3950(67)90278-X.

Busch, J., Meißner, T., Potthoff, A., Bleyl, S., Georgi, A., Mackenzie, K., Trabitzsch, R., Werban, U., and Oswald, S.E. 2015. A field investigation on transport of carbon-supported nanoscale zero-valent iron (nZVI) in groundwater. Journal of Contaminant Hydrology, **181**: 59–68. doi:10.1016/j.jconhyd.2015.03.009.

Carman, P.C. 1937. Fluid flow through granular beds. Transactions, Institution of Chemical Engineers (London)., **15**: 150–166.

Carman, P.C. 1956. Flow of gases through porous media. London : Butterworths Scientific. Available from https://trove.nla.gov.au/version/26415925 [accessed 29 April 2018].

Chowdhury, A.I.A., Krol, M.M., Kocur, C.M., Boparai, H.K., Weber, K.P., Sleep, B.E., and O'Carroll, D.M. 2015. nZVI injection into variably saturated soils: Field and modeling study. Journal of Contaminant Hydrology, **183**: 16–28. doi:10.1016/j.jconhyd.2015.10.003.

COMSOL User's Guide. 2017. Introduction to COMSOL Multiphysics. Available from https://cdn.comsol.com/documentation/5.3.0.260/IntroductionToCOMSOLMultiphysics.pdf [accessed 1 August 2017].

Costas, K., Knorr, R.S., and Condon, S.K. 2002. A case-control study of childhood leukemia in Woburn, Massachusetts: the relationship between leukemia incidence and exposure to public drinking water. The Science of the Total Environment, **300**(1–3): 23–35.

Cullen, E., M. O'Carroll, D., Yanful, E., and Sleep, B. 2010. Simulation of the subsurface mobility of carbon nanoparticles at the field scale. Advances in Water Resources, **33**: 361–371. doi:10.1016/j.advwatres.2009.12.001.

De Wiest, R.J.M. 1966. On the storage coefficient and the equations of groundwater flow. Journal of Geophysical Research, **71**(4): 1117–1122. doi:10.1029/JZ071i004p01117.

Dekker, T.J., and Abriola, L.M. 2000. The influence of field-scale heterogeneity on the infiltration and entrapment of dense nonaqueous phase liquids in saturated formations. Journal of Contaminant Hydrology, **42**(2–4): 187–218. doi:10.1016/S0169-7722(99)00092-3.

Dill, K.A. 1980. Concentration Dependence of the Viscosity and Viscoelasticity of Polymer Solutions: Application of the Theory of Muthukumar and Freed. doi:10.1021/ma60075a026.

Elliott, D.W., and Zhang, W. 2001. Field Assessment of Nanoscale Bimetallic Particles for Groundwater Treatment. Environmental Science & Technology, **35**(24): 4922–4926. doi:10.1021/es0108584.

Fetter, C.W., Boving, T., and Kreamer, D. 1993. Contaminant Hydrogeology: Third Edition. Waveland Press.

Frenzel, H. 1995. A field generator based on Mejia's algorithm. Institut fr Umweltphysik, University of Heidelberg,.

Frimmel, F.H., Kammer, F. von der, and Flemming, H.-C. (*Editors*). 2007. Colloidal Transport in Porous Media. Springer-Verlag, Berlin Heidelberg. Available from //www.springer.com/us/book/9783540713388 [accessed 26 November 2018].

Glazier, R., Venkatakrishnan, F., Gheorghiu, L., Walata, R.N., and Zhang, W. 2003. Nanotechnology takes root. Civil Engineering, **73**(5): 64–69.

Grunberg, L., and Nissan, A.H. 1949. Mixture Law for Viscosity. Nature, **164**(4175): 799–800. doi:10.1038/164799b0.

Harr, J. 1996. A civil action. Vintage Books, New York.

He, F., Zhang, M., Qian, T., and Zhao, D. 2009. Transport of carboxymethyl cellulose stabilized iron nanoparticles in porous media: column experiments and modeling. Journal of Colloid and Interface Science, **334**(1): 96–102. doi:10.1016/j.jcis.2009.02.058.

He, F., and Zhao, D. 2007. Manipulating the Size and Dispersibility of Zerovalent Iron Nanoparticles by Use of Carboxymethyl Cellulose Stabilizers. Environmental Science & Technology, **41**(17): 6216–6221. doi:10.1021/es0705543.

He, F., Zhao, D., and Paul, C. 2010. Field assessment of carboxymethyl cellulose stabilized iron nanoparticles for in situ destruction of chlorinated solvents in source zones. Water Research, **44**(7): 2360–2370. doi:10.1016/j.watres.2009.12.041.

Henn, K.W., and Waddill, D.W. 2006. Utilization of nanoscale zero-valent iron for source remediation—A case study. Remediation Journal, **16**(2): 57–77. doi:10.1002/rem.20081.

Johnson, R.L., Johnson, G.O., Nurmi, J.T., and Tratnyek, P.G. 2009. Natural Organic Matter Enhanced Mobility of Nano Zerovalent Iron. Environmental Science & Technology, **43**(14): 5455–5460. doi:10.1021/es900474f.

Jussel, P., Stauffer, F., and Dracos, T. 1994. Transport modeling in heterogeneous aquifers: 1. Statistical description and numerical generation of gravel deposits. Water Resources Research, **30**(6): 1803–1817. doi:10.1029/94WR00162.

Kanel, S.R., Nepal, D., Manning, B., and Choi, H. 2007. Transport of surface-modified iron nanoparticle in porous media and application to arsenic(III) remediation. Journal of Nanoparticle Research, **9**(5): 725–735. doi:10.1007/s11051-007-9225-7.

Kirkham, M.B. 2014. Principles of Soil and Plant Water Relations. Academic Press.

Köber, R., Hollert, H., Hornbruch, G., Jekel, M., Kamptner, A., Klaas, N., Maes, H., Mangold, K.-M., Martac, E., Matheis, A., Paar, H., Schäffer, A., Schell, H., Schiwy, A., Schmidt, K.R., Strutz, T.J., Thümmler, S., Tiehm, A., and Braun, J. 2014. Nanoscale zero-valent iron flakes for groundwater treatment. Environmental Earth Sciences, **72**(9): 1. doi:10.1007/s12665-014-3239-0.

Kocur, C. 2015. Field Scale Application of Nanoscale Zero Valent Iron: Mobility, Contaminant Degradation, and Impact on Microbial Communities. Electronic Thesis and Dissertation Repository,. Available from https://ir.lib.uwo.ca/etd/3068.

Kocur, C.M., Chowdhury, A.I., Sakulchaicharoen, N., Boparai, H.K., Weber, K.P., Sharma, P., Krol, M.M., Austrins, L., Peace, C., Sleep, B.E., and O'Carroll, D.M. 2014. Characterization of nZVI Mobility in a Field Scale Test. Environmental Science & Technology, **48**(5): 2862–2869. doi:10.1021/es4044209.

Kocur, C.M., O'Carroll, D.M., and Sleep, B.E. 2013. Impact of nZVI stability on mobility in porous media. Journal of Contaminant Hydrology, **145**: 17–25. doi:10.1016/j.jconhyd.2012.11.001.

Kozeny, J. 1927. Ueber kapillare Leitung des Wassers im Boden. Sitzungsber Akad. Wiss., Wien, **136(2a)**: 271–306.

Krol, M.M., Oleniuk, A.J., Kocur, C.M., Sleep, B.E., Bennett, P., Xiong, Z., and O'Carroll, D.M. 2013. A Field-Validated Model for In Situ Transport of

Polymer-Stabilized nZVI and Implications for Subsurface Injection. Environmental Science & Technology, **47**(13): 7332–7340. doi:10.1021/es3041412.

Laumann, S., Micić, V., Lowry, G.V., and Hofmann, T. 2013. Carbonate minerals in porous media decrease mobility of polyacrylic acid modified zero-valent iron nanoparticles used for groundwater remediation. Environmental Pollution, **179**: 53–60. doi:10.1016/j.envpol.2013.04.004.

Li, J., Bhattacharjee, S., and Ghoshal, S. 2015. The effects of viscosity of carboxymethyl cellulose on aggregation and transport of nanoscale zerovalent iron. Colloids and Surfaces A: Physicochemical and Engineering Aspects, **481**. doi:10.1016/j.colsurfa.2015.05.023.

Li, J., Rajajayavel, S.R.C., and Ghoshal, S. 2016. Transport of carboxymethyl cellulose-coated zerovalent iron nanoparticles in a sand tank: Effects of sand grain size, nanoparticle concentration and injection velocity. Chemosphere, **150**: 8–16. doi:10.1016/j.chemosphere.2015.12.075.

Li, X., Elliott, D.W., and Zhang, W. 2006. Zero-Valent Iron Nanoparticles for Abatement of Environmental Pollutants: Materials and Engineering Aspects. Critical Reviews in Solid State and Materials Sciences, **31**(4): 111–122. doi:10.1080/10408430601057611.

Lin, Y.H., Tseng, H.H., Wey, M.Y., and Lin, M.D. 2010. Characteristics of two types of stabilized nano zero-valent iron and transport in porous media. The Science of the total environment, **408**(10): 2260–2267. doi:10.1016/j.scitotenv.2010.01.039.

Mejía, J.M., and Rodríguez-Iturbe, I. 1974. On the synthesis of random field sampling from the spectrum: An application to the generation of hydrologic spatial processes. Water Resources Research, **10**(4): 705–711.

Mishra, P.C., Mukherjee, S., Nayak, S.K., and Panda, A. 2014. A brief review on viscosity of nanofluids. International Nano Letters, **4**(4): 109–120. doi:10.1007/s40089-014-0126-3.

Molnar, I.L., Johnson, W.P., Gerhard, J.I., Willson, C.S., and O'Carroll, D.M. 2015. Predicting colloid transport through saturated porous media: A critical review. Water Resources Research, **51**(9): 6804–6845. doi:10.1002/2015WR017318.

Mondal, P.K., Furbacher, P.D., Cui, Z., Krol, M.M., and Sleep, B.E. 2018. Transport of polymer stabilized nano-scale zero-valent iron in porous media. Journal of Contaminant Hydrology, **212**: 65–77. doi:10.1016/j.jconhyd.2017.11.004.

Montgomery, D.C., and Runger, G.C. 2007. Wiley: Applied Statistics and Probability for Engineers, 6e - Douglas C. Montgomery, George C. Runger. Available from http://ca.wiley.com/WileyCDA/WileyTitle/productCd-EHEP002914.html [accessed 15 July 2017].

National Research Council. 1999. Groundwater and soil cleanup: Improving management of persistent contaminants. National Academies Press.
Nelson, K.E., and Ginn, T.R. 2005. Colloid Filtration Theory and the Happel Sphere-in-Cell Model Revisited with Direct Numerical Simulation of Colloids. Langmuir, **21**(6): 2173–2184. doi:10.1021/la048404i.
O'Carroll, D., Sleep, B., Krol, M., Boparai, H., and Kocur, C. 2013. Nanoscale zero valent iron and bimetallic particles for contaminated site remediation. Adv. Advances in Water Resources, **51**: 104–122. doi:10.1016/j.advwatres.2012.02.005.
Petosa, A.R., Jaisi, D.P., Quevedo, I.R., Elimelech, M., and Tufenkji, N. 2010. Aggregation and Deposition of Engineered Nanomaterials in Aquatic Environments: Role of Physicochemical Interactions. Environmental Science & Technology, **44**(17): 6532–6549. doi:10.1021/es100598h.
Phenrat, T., Cihan, A., Kim, H.-J., Mital, M., Illangasekare, T., and Lowry, G.V. 2010. Transport and Deposition of Polymer-Modified Fe0 Nanoparticles in 2-D Heterogeneous Porous Media: Effects of Particle Concentration, Fe0 Content, and Coatings. Environmental Science & Technology, **44**(23): 9086–9093. doi:10.1021/es102398e.
Phenrat, T., Kim, H.-J., Fagerlund, F., Illangasekare, T., Tilton, R.D., and Lowry, G.V. 2009. Particle size distribution, concentration, and magnetic attraction affect transport of polymer-modified Fe(0) nanoparticles in sand columns. Environmental Science & Technology, **43**(13): 5079–5085.
Phenrat, T., Saleh, N., Sirk, K., Tilton, R.D., and Lowry, G.V. 2007. Aggregation and Sedimentation of Aqueous Nanoscale Zerovalent Iron Dispersions. Environmental Science & Technology, **41**(1): 284–290. doi:10.1021/es061349a.
Quinn, J., Geiger, C., Clausen, C., Brooks, K., Coon, C., O'Hara, S., Krug, T., Major, D., Yoon, W.-S., Gavaskar, A., and Holdsworth, T. 2005. Field Demonstration of DNAPL Dehalogenation Using Emulsified Zero-Valent Iron. Environmental Science & Technology, **39**(5): 1309–1318. doi:10.1021/es0490018.
Raychoudhury, T., Naja, G., and Ghoshal, S. 2010. Assessment of transport of two polyelectrolyte-stabilized zero-valent iron nanoparticles in porous media. Journal of contaminant hydrology, **118**(3–4): 143–151. doi:10.1016/j.jconhyd.2010.09.005.
Raychoudhury, T., Tufenkji, N., and Ghoshal, S. 2012. Aggregation and deposition kinetics of carboxymethyl cellulose-modified zero-valent iron nanoparticles in porous media. Water Research, **46**(6): 1735–1744. doi:10.1016/j.watres.2011.12.045.
Raychoudhury, T., Tufenkji, N., and Ghoshal, S. 2014. Straining of polyelectrolyte-stabilized nanoscale zero valent iron particles during

transport through granular porous media. Water Research, **50**: 80–89. doi:10.1016/j.watres.2013.11.038.
Rudolph, D.L., Cherry, J.A., and Farvolden, R.N. 1991. Groundwater Flow and Solute Transport in Fractured Lacustrine Clay Near Mexico City. Water Resources Research, **27**(9): 2187–2201. doi:10.1029/91WR01306.
Sakulchaicharoen, N., O'Carroll, D.M., and Herrera, J.E. 2010. Enhanced stability and dechlorination activity of pre-synthesis stabilized nanoscale FePd particles. Journal of Contaminant Hydrology, **118**(3–4): 117–127. doi:10.1016/j.jconhyd.2010.09.004.
Schijven, J.F., and Hassanizadeh, S.M. 2000. Removal of Viruses by Soil Passage: Overview of Modeling, Processes, and Parameters. Critical Reviews in Environmental Science and Technology, **30**(1): 49–127. doi:10.1080/10643380091184174.
Schijven, J.F., and Šimůnek, J. 2002. Kinetic modeling of virus transport at the field scale. Journal of Contaminant Hydrology, **55**: 113–135. doi:10.1016/S0169-7722(01)00188-7.
Sleep, B.E., and Sykes, J.F. 1993. Compositional simulation of groundwater contamination by organic compounds: 1. Model development and verification. Water Resources Research, **29**(6): 1697–1708. doi:10.1029/93WR00283.
Snedecor, G.W., and Cochran, W.G. 1980. Statistical methods, 7thEdn. Ames: Iowa State Univ. Press Iowa,: 180.
Spiegel, M.R. 1992. Shaum's outline of theory and problems of probability and statistics, 2nd Edn. McGraw-Hill.
Steefel, C.I., and Lasaga, A.C. 1992. Putting transport into water-rock interaction models. Geology, **20**(8): 680–684. doi:10.1130/0091-7613(1992)020<0680:PTIWRI>2.3.CO;2.
Strutz, T.J., Hornbruch, G., Dahmke, A., and Köber, R. 2016. Influence of permeability on nanoscale zero-valent iron particle transport in saturated homogeneous and heterogeneous porous media. Environmental Science and Pollution Research International, **23**(17): 17200–17209. doi:10.1007/s11356-016-6814-y.
Su, C., Puls, R.W., Krug, T.A., Watling, M.T., O'Hara, S.K., Quinn, J.W., and Ruiz, N.E. 2013. Travel distance and transformation of injected emulsified zerovalent iron nanoparticles in the subsurface during two and half years. Water Research, **47**(12): 4095–4106. doi:10.1016/j.watres.2012.12.042.
Sudicky, E.A. 1986. A natural gradient experiment on solute transport in a sand aquifer: Spatial variability of hydraulic conductivity and its role in the dispersion process. Water Resources Research, **22**(13): 2069–2082. doi:10.1029/WR022i013p02069.
Taghavy, A., Costanza, J., Pennell, K.D., and Abriola, L.M. 2010. Effectiveness of nanoscale zero-valent iron for treatment of a PCE-DNAPL source zone.

Journal of Contaminant Hydrology, **118**(3–4): 128–142. doi:10.1016/j.jconhyd.2010.09.001.
Tiraferri, A., and Sethi, R. 2008. Enhanced transport of zerovalent iron nanoparticles in saturated porous media by guar gum. Journal of Nanoparticle Research, **11**(3): 635. doi:10.1007/s11051-008-9405-0.
Tufenkji, N. 2007. Modeling Microbial Transport in Porous Media: Traditional Approaches and Recent Developments. Advances in Water Resources, **30**: 1455–1469. doi:10.1016/j.advwatres.2006.05.014.
Tufenkji, N., and Elimelech, M. 2004. Correlation Equation for Predicting Single-Collector Efficiency in Physicochemical Filtration in Saturated Porous Media. Environmental Science & Technology, **38**(2): 529–536. doi:10.1021/es034049r.
Velimirovic, M., Tosco, T., Uyttebroek, M., Luna, M., Gastone, F., De Boer, C., Klaas, N., Sapion, H., Eisenmann, H., Larsson, P.-O., Braun, J., Sethi, R., and Bastiaens, L. 2014. Field assessment of guar gum stabilized microscale zerovalent iron particles for in-situ remediation of 1,1,1-trichloroethane. Journal of Contaminant Hydrology, **164**: 88–99. doi:10.1016/j.jconhyd.2014.05.009.
Wang, L.K., Chen, J.P., Hung, Y.-T., and Shammas, N.K. 2009. Heavy Metals in the Environment. CRC Press.
Wei, Y.-T., Wu, S.-C., Chou, C.-M., Che, C.-H., Tsai, S.-M., and Lien, H.-L. 2010. Influence of nanoscale zero-valent iron on geochemical properties of groundwater and vinyl chloride degradation: A field case study. Water Research, **44**(1): 131–140. doi:10.1016/j.watres.2009.09.012.
Woodbury, A.D., and Sudicky, E.A. 1991. The geostatistical characteristics of the borden aquifer. Water Resources Research, **27**(4): 533–546. doi:10.1029/90WR02545.
Yang, G.C.C., Tu, H.-C., and Hung, C.-H. 2007. Stability of nanoiron slurries and their transport in the subsurface environment. Separation and Purification Technology, **58**(1): 166–172. doi:10.1016/j.seppur.2007.07.018.
Yao, K.-M., Habibian, M.T., and O'Melia, C.R. 1971. Water and waste water filtration. Concepts and applications. Environmental Science & Technology, **5**(11): 1105–1112. doi:10.1021/es60058a005.
Zhang, W. 2003. Nanoscale Iron Particles for Environmental Remediation: An Overview. Journal of Nanoparticle Research, **5**(3–4): 323–332. doi:10.1023/A:1025520116015.

Appendix A

Table A. 1: Case 1: Simulated values at 48 hours for Borden aquifer

Realization number	XCN (m)	XNSP (m)	ZCN (m)	ZNSP (m)	SS (mol/kg)
7	9.94	1.68	9.50	1.92	5.91E-03
15	10.43	1.88	11.49	1.72	5.93E-03
20	10.24	1.82	11.27	1.84	5.95E-03
26	9.64	2.18	10.86	1.51	5.93E-03
33	10.27	2.16	10.75	1.61	5.93E-03
41	10.22	2.29	11.17	1.53	5.92E-03
49	9.77	1.80	10.58	1.70	5.94E-03
56	10.20	1.56	10.89	1.49	5.95E-03
65	10.00	2.36	11.01	1.22	5.95E-03
73	10.17	1.72	10.50	1.84	5.94E-03
77	10.10	2.08	10.78	1.48	5.94E-03
86	10.21	1.76	10.75	1.95	5.93E-03
89	10.43	2.31	11.03	1.21	5.95E-03
93	10.26	1.36	10.81	1.67	5.95E-03
99	10.26	2.01	11.72	1.40	5.95E-03

Table A. 2: Case 2: Simulated values at 48 hours for Borden aquifer

Realization number	XCN (m)	XNSP (m)	ZCN (m)	ZNSP (m)	SS (mol/kg)
7	10.00	1.67	9.51	1.92	5.91E-03
15	10.49	1.90	11.50	1.72	5.93E-03
20	10.30	1.83	11.27	1.83	5.94E-03
26	9.70	2.16	10.86	1.52	5.93E-03
33	10.33	2.17	10.76	1.61	5.93E-03
41	10.28	2.29	11.17	1.52	5.92E-03
49	9.81	1.81	10.57	1.70	5.94E-03
56	10.22	1.57	10.89	1.49	5.95E-03
65	10.05	2.36	11.01	1.22	5.95E-03
73	10.21	1.72	10.50	1.84	5.94E-03
77	10.15	2.08	10.77	1.48	5.94E-03
86	10.25	1.76	10.76	1.95	5.93E-03
89	10.47	2.33	11.03	1.20	5.95E-03
93	10.28	1.37	10.82	1.66	5.95E-03
99	10.31	2.02	11.72	1.40	5.95E-03

Table A. 3: Case 3: Simulated values at 48 hours for Borden aquifer

Realization number	XCN (m)	XNSP (m)	ZCN (m)	ZNSP (m)	SS (mol/kg)
7	10.27	1.65	9.64	1.78	5.90E-03
15	10.78	2.00	11.51	1.70	5.93E-03
20	10.62	1.87	11.24	1.79	5.93E-03
26	9.99	2.08	10.85	1.53	5.92E-03
33	10.63	2.23	10.79	1.55	5.93E-03
41	10.61	2.34	11.13	1.48	5.91E-03
49	10.03	1.83	10.58	1.68	5.93E-03
56	10.34	1.59	10.90	1.47	5.95E-03
65	10.31	2.36	11.01	1.22	5.94E-03
73	10.45	1.73	10.52	1.80	5.93E-03
77	10.39	2.11	10.77	1.45	5.93E-03
86	10.50	1.77	10.78	1.93	5.92E-03
89	10.69	2.40	11.02	1.17	5.94E-03
93	10.40	1.39	10.82	1.65	5.95E-03
99	10.53	2.07	11.70	1.38	5.95E-03

Table A. 4: Case 4: Simulated values at 48 hours for Borden aquifer

Realization number	XCN (m)	XNSP (m)	ZCN (m)	ZNSP (m)	SS (mol/kg)
7	9.94	1.68	9.50	1.92	1.53E-02
15	10.43	1.88	11.49	1.72	1.54E-02
20	10.24	1.82	11.27	1.84	1.54E-02
26	9.64	2.17	10.86	1.51	1.53E-02
33	10.27	2.15	10.76	1.61	1.54E-02
41	10.22	2.28	11.17	1.52	1.53E-02
49	9.76	1.80	10.58	1.70	1.54E-02
56	10.20	1.56	10.89	1.49	1.54E-02
65	10.00	2.36	11.01	1.22	1.54E-02
73	10.17	1.71	10.50	1.84	1.54E-02
77	10.10	2.07	10.78	1.47	1.54E-02
86	10.21	1.76	10.76	1.95	1.53E-02
89	10.43	2.31	11.03	1.20	1.54E-02
93	10.26	1.36	10.81	1.66	1.54E-02
99	10.26	2.01	11.72	1.40	1.54E-02

Table A. 5: Case 5: Simulated values at 48 hours for Borden aquifer

Realization number	XCN (m)	XNSP (m)	ZCN (m)	ZNSP (m)	SS (mol/kg)
7	9.93	1.56	9.44	1.80	6.21E-01
15	10.46	1.79	11.54	1.61	6.22E-01
20	10.27	1.70	11.30	1.74	6.22E-01
26	9.65	2.00	10.85	1.36	6.23E-01
33	10.28	2.00	10.81	1.44	6.23E-01
41	10.27	2.20	11.17	1.34	6.23E-01
49	9.76	1.67	10.63	1.56	6.23E-01
56	10.20	1.42	10.88	1.36	6.24E-01
65	9.97	2.23	11.00	1.10	6.24E-01
73	10.16	1.54	10.51	1.73	6.22E-01
77	10.09	1.93	10.80	1.31	6.23E-01
86	10.20	1.60	10.80	1.83	6.22E-01
89	10.50	2.25	11.03	1.02	6.24E-01
93	10.25	1.22	10.83	1.58	6.22E-01
99	10.28	1.91	11.71	1.28	6.23E-01

Table A. 6: Case 6: Simulated values at 48 hours for Borden aquifer

Realization number	XCN (m)	XNSP (m)	ZCN (m)	ZNSP (m)	SS (mol/kg)
7.00	9.95	2.49	9.32	2.75	5.52E-03
15.00	10.54	2.70	11.54	2.42	5.60E-03
20.00	10.22	2.68	11.31	2.57	5.58E-03
26.00	9.61	2.98	10.93	2.22	5.55E-03
33.00	10.29	2.95	10.56	2.33	5.54E-03
41.00	10.11	3.01	11.30	2.34	5.49E-03
49.00	9.77	2.60	10.37	2.48	5.62E-03
56.00	10.22	2.43	10.94	2.34	5.75E-03
65.00	10.10	3.22	11.16	1.88	5.65E-03
73.00	10.16	2.62	10.37	2.60	5.57E-03
77.00	10.18	2.91	10.84	2.30	5.55E-03
86.00	10.25	2.60	10.55	2.58	5.55E-03
89.00	10.39	3.02	11.05	2.09	5.66E-03
93.00	10.37	2.26	10.81	2.50	5.77E-03
99.00	10.30	2.85	12.00	2.15	5.68E-03

Table A. 7: Case A: Simulated values at 48 hours for Borden aquifer

Realization number	XCN (m)	XNSP (m)	ZCN (m)	ZNSP (m)	SS (mol/kg)
7	9.82	1.76	9.04	2.00	2.53E-04
15	10.78	1.95	11.92	1.46	3.03E-04
20	10.40	2.03	11.73	1.74	2.79E-04
26	9.49	2.13	10.91	1.31	4.52E-04
33	10.43	2.28	10.72	1.57	3.60E-04
41	10.40	2.46	11.30	1.40	3.57E-04
49	9.65	1.82	10.43	1.71	2.91E-04
56	10.31	1.59	11.07	1.51	1.96E-04
65	9.99	2.51	11.08	1.00	3.56E-04
73	10.32	1.81	10.58	1.91	2.84E-04
77	10.20	2.14	10.82	1.33	3.68E-04
86	10.36	1.71	10.82	1.98	3.63E-04
89	10.7	2.3	11.1	9.7E-1	3.16E-04
93	10.4	1.5	11.1	1.81	1.46E-04
99	10.5	2.1	11.9	1.19	2.72E-04

Table A. 8: Case B: Simulated values at 48 hours for Borden aquifer

Realization number	XCN (m)	XNSP (m)	ZCN (m)	ZNSP (m)	SS (mol/kg)
7	9.90	1.69	9.29	1.95	6.57E-04
15	10.59	1.89	11.71	1.60	7.34E-04
20	10.32	1.88	11.50	1.81	6.94E-04
26	9.58	2.12	10.88	1.41	9.80E-04
33	10.33	2.17	10.75	1.58	8.37E-04
41	10.30	2.34	11.24	1.45	8.26E-04
49	9.70	1.80	10.52	1.70	7.18E-04
56	10.26	1.57	10.98	1.50	5.64E-04
65	9.99	2.41	11.05	1.10	8.02E-04
73	10.24	1.73	10.54	1.86	7.35E-04
77	10.14	2.07	10.79	1.40	8.65E-04
86	10.28	1.72	10.79	1.96	8.36E-04
89	10.57	2.33	11.05	1.09	7.55E-04
93	10.34	1.42	10.94	1.75	4.67E-04
99	10.37	2.05	11.85	1.29	6.70E-04

Table A. 9: Case C: Simulated values at 48 hours for Borden aquifer

Realization number	XCN (m)	XNSP (m)	ZCN (m)	ZNSP (m)	SS (mol/kg)
7	9.94	1.60	9.47	1.82	1.04E-03
15	10.46	1.79	11.56	1.62	1.13E-03
20	10.28	1.73	11.34	1.77	1.08E-03
26	9.64	2.05	10.86	1.41	1.37E-03
33	10.28	2.05	10.78	1.52	1.23E-03
41	10.26	2.20	11.17	1.41	1.23E-03
49	9.74	1.72	10.59	1.63	1.11E-03
56	10.22	1.51	10.92	1.45	9.48E-04
65	9.98	2.27	11.01	1.14	1.21E-03
73	10.19	1.62	10.53	1.78	1.13E-03
77	10.10	1.97	10.77	1.38	1.26E-03
86	10.23	1.65	10.79	1.89	1.23E-03
89	10.47	2.24	11.04	1.10	1.16E-03
93	10.29	1.33	10.87	1.65	8.31E-04
99	10.29	1.94	11.75	1.30	1.05E-03

Table A. 10: Case 1: Simulated values at 48 hours for Swiss aquifer

Realization number	XCN (m)	XNSP (m)	ZCN (m)	ZNSP (m)	SS (mol/kg)
7	9.65	2.32	8.28	2.05	5.82E-03
15	11.50	2.86	12.26	1.51	5.92E-03
20	10.49	2.76	11.97	1.75	5.95E-03
26	8.94	3.00	11.04	1.34	5.88E-03
33	10.86	3.13	10.95	1.38	5.90E-03
41	10.89	3.55	11.55	1.30	5.79E-03
49	9.38	2.23	10.68	1.56	5.95E-03
56	10.44	1.66	11.22	1.30	5.98E-03
65	9.82	3.63	11.20	1.00	5.94E-03
73	10.31	1.98	10.54	2.01	5.95E-03
77	10.35	2.92	10.99	1.27	5.92E-03
86	10.41	2.17	11.06	2.04	5.92E-03
89	11.62	3.50	11.10	0.84	5.81E-03
93	10.40	1.24	11.20	1.57	5.97E-03
99	10.80	2.85	12.24	1.22	5.99E-03

Table A. 11: Case 2: Simulated values at 48 hours for Swiss aquifer

Realization number	XCN (m)	XNSP (m)	ZCN (m)	ZNSP (m)	SS (mol/kg)
7	9.92	2.23	8.32	2.03	5.81E-03
15	11.63	2.88	12.27	1.51	5.91E-03
20	10.70	2.75	11.96	1.75	5.94E-03
26	9.05	2.96	11.04	1.35	5.88E-03
33	10.97	3.15	10.96	1.37	5.90E-03
41	11.04	3.53	11.54	1.30	5.77E-03
49	9.46	2.27	10.67	1.56	5.94E-03
56	10.46	1.66	11.22	1.30	5.98E-03
65	9.91	3.63	11.20	1.00	5.94E-03
73	10.39	1.97	10.55	2.00	5.95E-03
77	10.45	2.95	10.99	1.27	5.91E-03
86	10.48	2.16	11.06	2.04	5.92E-03
89	11.67	3.50	11.09	0.84	5.79E-03
93	10.43	1.24	11.20	1.57	5.97E-03
99	10.88	2.86	12.24	1.21	5.99E-03

Table A. 12: Case 3: Simulated values at 48 hours for Swiss aquifer

Realization number	XCN (m)	XNSP (m)	ZCN (m)	ZNSP (m)	SS (mol/kg)
7	10.63	2.02	9.01	1.59	5.82E-03
15	12.21	2.90	12.27	1.51	5.84E-03
20	11.68	2.64	11.82	1.66	5.85E-03
26	9.68	2.65	11.03	1.39	5.87E-03
33	11.47	3.21	11.06	1.21	5.85E-03
41	11.72	3.39	11.41	1.19	5.60E-03
49	9.71	2.30	10.74	1.47	5.91E-03
56	10.57	1.70	11.23	1.28	5.98E-03
65	10.39	3.54	11.21	1.00	5.92E-03
73	10.77	1.96	10.59	1.92	5.94E-03
77	10.89	2.97	10.97	1.24	5.89E-03
86	10.89	2.15	11.11	1.98	5.89E-03
89	11.94	3.48	11.08	0.82	5.65E-03
93	10.53	1.29	11.21	1.56	5.97E-03
99	11.25	2.88	12.21	1.18	5.96E-03

Table A. 13: Case 4: Simulated values at 48 hours for Swiss aquifer

Realization number	XCN (m)	XNSP (m)	ZCN (m)	ZNSP (m)	SS (mol/kg)
7	9.65	2.32	8.28	2.05	1.51E-02
15	11.51	2.86	12.26	1.51	1.53E-02
20	10.49	2.76	11.97	1.75	1.54E-02
26	8.94	3.00	11.04	1.34	1.52E-02
33	10.86	3.12	10.95	1.37	1.53E-02
41	10.90	3.55	11.55	1.29	1.50E-02
49	9.38	2.23	10.68	1.55	1.54E-02
56	10.44	1.65	11.22	1.30	1.55E-02
65	9.82	3.63	11.20	0.99	1.54E-02
73	10.31	1.97	10.54	2.01	1.54E-02
77	10.35	2.92	10.99	1.27	1.53E-02
86	10.41	2.16	11.06	2.03	1.53E-02
89	11.62	3.50	11.10	0.84	1.50E-02
93	10.40	1.23	11.20	1.57	1.55E-02
99	10.80	2.85	12.24	1.22	1.55E-02

Table A. 14: Case 5: Simulated values at 48 hours for Swiss aquifer

Realization number	XCN (m)	XNSP (m)	ZCN (m)	ZNSP (m)	SS (mol/kg)
7	9.57	2.32	8.22	2.02	6.14E-01
15	11.73	2.91	12.28	1.39	6.22E-01
20	10.54	2.85	12.04	1.63	6.23E-01
26	8.94	2.85	11.02	1.19	6.20E-01
33	10.99	3.04	11.02	1.17	6.23E-01
41	11.12	3.55	11.47	1.12	6.13E-01
49	9.33	2.12	10.75	1.40	6.23E-01
56	10.43	1.55	11.17	1.19	6.26E-01
65	9.73	3.54	11.19	0.90	6.24E-01
73	10.31	1.83	10.58	1.91	6.22E-01
77	10.44	2.91	11.02	1.10	6.23E-01
86	10.40	2.05	11.17	1.91	6.22E-01
89	11.85	3.40	11.06	0.72	6.05E-01
93	10.37	1.15	11.24	1.52	6.23E-01
99	10.91	2.76	12.15	1.12	6.24E-01

Table A. 15: Case 6: Simulated values at 48 hours for Swiss aquifer

Realization number	XCN (m)	XNSP (m)	ZCN (m)	ZNSP (m)	SS (mol/kg)
7	9.81	3.11	8.03	2.49	5.26E-03
15	11.50	3.45	12.34	2.07	5.47E-03
20	10.42	3.36	11.93	2.38	5.45E-03
26	8.99	3.63	11.16	1.93	5.40E-03
33	10.78	3.68	10.68	2.02	5.40E-03
41	10.52	3.99	11.85	1.98	5.18E-03
49	9.43	2.93	10.31	2.28	5.58E-03
56	10.60	2.57	11.42	2.01	5.84E-03
65	10.03	4.31	11.36	1.42	5.56E-03
73	10.26	2.83	10.28	2.67	5.49E-03
77	10.47	3.57	11.10	2.01	5.43E-03
86	10.45	2.92	10.67	2.52	5.44E-03
89	10.45	2.92	10.67	2.52	5.44E-03
93	10.66	2.18	11.26	2.39	5.85E-03
99	10.80	3.68	12.76	1.76	5.59E-03

Table A. 16: Case A: Simulated values at 48 hours for Swiss aquifer

Realization number	XCN (m)	XNSP (m)	ZCN (m)	ZNSP (m)	SS (mol/kg)
7	9.41	2.37	7.66	1.82	3.20E-04
15	12.09	2.76	12.55	1.09	4.23E-04
20	10.77	3.08	12.47	1.33	3.36E-04
26	8.61	2.88	11.04	1.09	6.49E-04
33	11.33	3.26	10.91	1.28	5.07E-04
41	11.42	3.75	11.56	1.15	5.37E-04
49	9.27	2.22	10.49	1.60	3.23E-04
56	10.66	1.70	11.53	1.29	1.65E-04
65	9.8	3.7	11.2	8E-01	5.21E-04
73	10.61	2.13	10.73	2.10	3.25E-04
77	10.71	3.07	11.04	1.07	4.95E-04
86	10.64	1.99	11.16	2.04	4.79E-04
89	12.23	3.27	11.04	6E-01	4.53E-04
93	10.77	1.58	11.93	1.65	6.89E-05
99	11.23	2.80	12.25	1.04	3.91E-04

Table A. 17: Case B: Simulated values at 48 hours for Swiss aquifer

Realization number	XCN (m)	XNSP (m)	ZCN (m)	ZNSP (m)	SS (mol/kg)
7	9.55	2.25	7.96	1.93	7.13E-04
15	11.83	2.80	12.47	1.27	8.26E-04
20	10.66	2.86	12.28	1.56	7.14E-04
26	8.81	2.90	11.04	1.21	1.20E-03
33	11.06	3.15	10.95	1.31	9.83E-04
41	11.17	3.61	11.56	1.20	1.03E-03
49	9.28	2.20	10.61	1.57	7.24E-04
56	10.56	1.68	11.40	1.29	4.73E-04
65	9.80	3.64	11.20	9E-01	1.02E-03
73	10.45	2.01	10.65	2.05	7.62E-04
77	10.49	2.94	11.00	1.15	9.85E-04
86	10.52	2.05	11.13	2.03	9.51E-04
89	11.97	3.40	11.07	7E-01	8.85E-04
93	10.59	1.42	11.62	1.67	2.53E-04
99	11.02	2.82	12.26	1.12	8.07E-04

Table A. 18: Case C: Simulated values at 48 hours for Swiss aquifer

Realization number	XCN (m)	XNSP (m)	ZCN (m)	ZNSP (m)	SS (mol/kg)
7	9.64	2.13	8.25	1.92	1.06E-03
15	11.59	2.72	12.34	1.37	1.17E-03
20	10.60	2.65	12.10	1.64	1.06E-03
26	8.94	2.82	11.03	1.24	1.56E-03
33	10.89	3.01	10.99	1.28	1.36E-03
41	11.05	3.45	11.51	1.18	1.43E-03
49	9.32	2.13	10.71	1.49	1.11E-03
56	10.48	1.61	11.29	1.26	8.23E-04
65	9.78	3.50	11.20	9E-01	1.39E-03
73	10.37	1.87	10.62	1.94	1.16E-03
77	10.35	2.79	10.97	1.17	1.40E-03
86	10.45	2.01	11.13	1.98	1.31E-03
89	11.77	3.39	11.08	8E-01	1.27E-03
93	10.47	1.27	11.40	1.61	5.27E-04
99	10.88	2.72	12.22	1.13	1.16E-03

JOHN WILEY AND SONS LICENSE TERMS AND CONDITIONS

Jul 26, 2018

This Agreement between Mr. MD ABDULLAH ASAD ("You") and John Wiley and Sons ("John Wiley and Sons") consists of your license details and the terms and conditions provided by John Wiley and Sons and Copyright Clearance Center.

License Number	4396781066037
License date	Jul 26, 2018
Licensed Content Publisher	John Wiley and Sons
Licensed Content Publication	Water Resources Research
Licensed Content Title	Predicting colloid transport through saturated porous media: A critical review
Licensed Content Author	Ian L. Molnar, William P. Johnson, Jason I. Gerhard, et al
Licensed Content Date	Sep 2, 2015
Licensed Content Volume	51
Licensed Content Issue	9
Licensed Content Pages	42
Type of use	Dissertation/Thesis
Requestor type	University/Academic
Format	Print and electronic
Portion	Figure/table
Number of figures/tables	1
Original Wiley figure/table number(s)	Figure 3
Will you be translating?	No
Title of your thesis / dissertation	TRANSPORT OF NANO SCALE ZERO VALENT IRON IN HETEROGENEOUS SOILS: MODEL DEVELOPMENT AND SENSITIVITY STUDY
Expected completion date	Dec 2018
Expected size (number of pages)	150
Requestor Location	Mr. MD ABDULLAH ASAD 360 ASSINIBOINE RD TORONTO, ON M3J1L3 Canada Attn: Mr. MD ABDULLAH ASAD
Publisher Tax ID	EU826007151
Total	0.00 CAD

Figure A.0.1: Proof of permission from Molnar et. al. (2015) and John Wiley and Sons to use Figure 3 of Molnar et. al. (2015) (Figure 2.1 in this thesis)